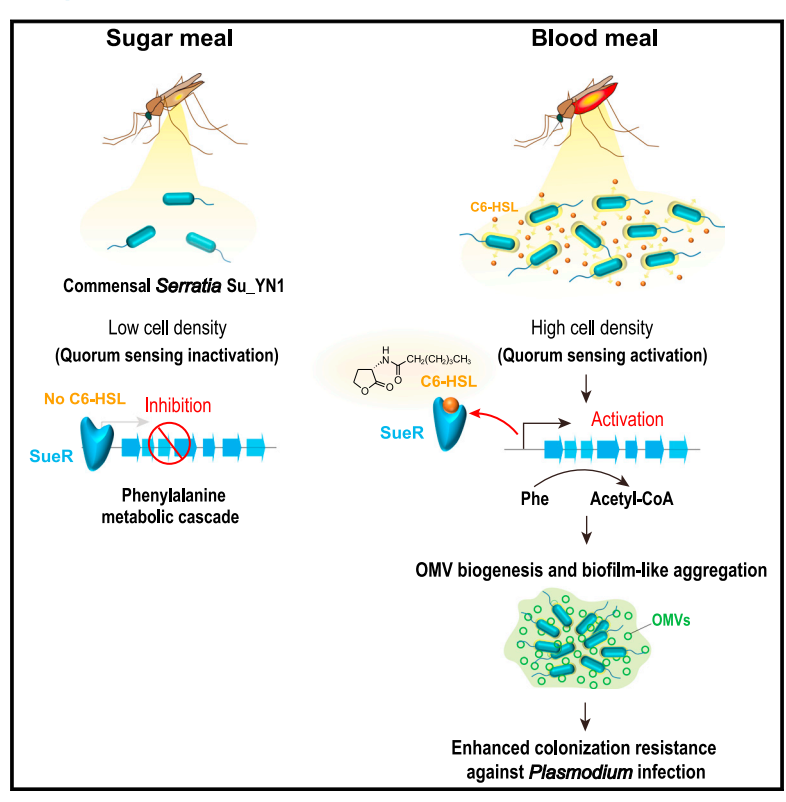
Quorum sensing-activated phenylalanine metabolism drives OMV biogenesis to enhance mosquito commensal colonization resistance to *Plasmodium*

Graphical abstract



Authors

Yongmao Jiang, Han Gao, Lihua Wang, Wenqian Hu, Guandong Wang, Sibao Wang

Correspondence

sbwang@cemps.ac.cn

In brief

Jiang et al. reveal that blood meal activates the mosquito symbiotic bacterium *Serratia ureilytica* Su_YN1 quorum sensing system, inducing the synthesis of C6-HSL molecules that drive OMV biogenesis by activating phenylalanine metabolism. This promotes bacterial biofilm-like aggregate formation, enhancing Su_YN1 gut colonization and its resistance to *Plasmodium*.

Highlights

- A quorum sensing circuit controls commensal gut colonization via OMV-mediated aggregation
- The C6-HSL quorum sensing molecule controls a phenylalanine metabolic cascade
- Metabolic conversion of phenylalanine to acetyl-CoA drives OMV biogenesis
- Exposing Anopheles to C6-HSL increases commensal colonization resistance to Plasmodium







Article

Quorum sensing-activated phenylalanine metabolism drives OMV biogenesis to enhance mosquito commensal colonization resistance to *Plasmodium*

Yongmao Jiang, 1,2,3 Han Gao, 1,2,3 Lihua Wang, 1,2 Wenqian Hu, 1,2 Guandong Wang, 1,2 and Sibao Wang 1,2,4,*

¹CAS Key Laboratory of Insect Developmental and Evolutionary Biology, CAS Center for Excellence in Molecular Plant Sciences, Shanghai Institute of Plant Physiology and Ecology, Chinese Academy of Sciences, Shanghai, China

²CAS Center for Excellence in Biotic Interactions, University of Chinese Academy of Sciences, Beijing, China

SUMMARY

Gut microbiota and its symbiotic relationship with the host are crucial for preventing pathogen infection. However, little is known about the mechanisms that drive commensal colonization. *Serratia* bacteria, commonly found in *Anopheles* mosquitoes, potentially mediate mosquito resistance to *Plasmodium*. Using *S. ureilytica* Su_YN1 as a model, we show that a quorum sensing (QS) circuit is crucial for stable colonization. After blood ingestion, the QS synthase Suel generates the signaling molecule N-hexanoyl-L-homoserine lactone (C6-HSL). Once C6-HSL binds to the QS receptor SueR, repression of the phenylalanine-to-acetyl-coenzyme A (CoA) conversion pathway is lifted. This pathway regulates outer membrane vesicle (OMV) biogenesis and promotes *Serratia* biofilm-like aggregate formation, facilitating gut adaptation and colonization. Notably, exposing *Serratia* Su_YN1-carrying *Anopheles* mosquitoes to C6-HSL increases *Serratia* gut colonization and enhances *Plasmodium* transmission-blocking efficacy. These findings provide insights into OMV biogenesis and commensal gut colonization and identify a powerful strategy for enhancing commensal resistance to pathogens.

INTRODUCTION

The gut microbiota has co-evolved with the host in a symbiotic relationship and plays a crucial role in host health and disease. ¹⁻⁴ The regulation of gut microbiota homeostasis has mainly been studied from the perspective of host immune regulation. To establish and colonize the host gut, commensal microbiota must overcome several physiological and biological stressors. ^{5,6} Moreover, both commensal and pathogenic microorganisms have evolved mechanisms to survive and persist in an unfavorable environment. ⁷ In addition, the microbiota is challenged by various intrinsic and extrinsic factors, such as diet, pathogen infections, and microbial interaction, ⁸ which can impact its composition and function. Despite extensive research on the mechanisms employed by intestinal pathogens to endure and survive in the intestinal tract, ^{9,10} little is known about the colonization and persistence mechanisms employed by gut commensals.

Mosquitoes are vectors of pathogens that cause numerous devastating infectious diseases such as malaria, Zika, dengue, and yellow fever, which pose a heavy burden on global public health. As pathogens are ingested with a blood meal, the vector gut microbiota plays a key role in modulating the outcome of

pathogen infection and transmission.¹¹ Certain symbiotic microbes mediate resistance against pathogen infection.¹ A promising strategy for blocking transmission of mosquito-transmitted diseases is to populate mosquitoes with anti-pathogen bacteria, known as paratransgenesis or symbiont-based transmission blocking strategy.^{1,8} However, the inhibition of *Plasmodium* by gut bacteria in the mosquito gut is dose-dependent.¹² Therefore, to successfully implement this strategy in the field, it is important to develop means to promote the effective colonization abundance of anti-pathogen bacteria in the harsh gut environment of blood-fed mosquitoes.¹³

Microbial symbiosis is a widespread biological phenomenon and is particularly common in arthropods, ¹⁴ yet the molecular mechanisms that drive stable colonization and persistence remain largely unknown. ⁵ Different from other insects such as fruit flies and bees that have a relatively simple and stable commensal community, the microbiota of hematophagous insects is highly complex and dynamic. ¹⁵ One reason for this diversity stems from the fact that hematophagous insects, including mosquitoes and ticks, depend on blood ingestion for propagation, and blood digestion produces oxidative stress on gut bacteria. ¹⁶ Recently, several bacteria, such as *Serratia* spp., ^{17–20} *Pantoea* spp., ²¹ and *Asaia* spp., ²¹ were found to



³These authors contributed equally

⁴Lead contact

^{*}Correspondence: sbwang@cemps.ac.cn https://doi.org/10.1016/j.chom.2023.08.017



stably colonize both field-caught and lab-reared *Anopheles* mosquitoes, indicating that these bacteria have evolved to adapt to the mosquito gut microenvironment. However, mechanisms underlying microbial symbiosis and adaptation remain to be explored.

Here, we show that the acyl-homoserine lactone (AHL)-type quorum sensing (QS) circuit is critical for stable colonization of *Serratia ureilytica* Su_YN1, a *Plasmodium*-blocking bacterium isolated from the field-caught mosquito, which directly kills *Plasmodium* development via the secretion of an antimalarial lipase. ¹⁷ We identified the N-hexanoyl-L-homoserine lactone (C6-HSL) QS signal molecule as a key factor driving *Serratia* colonization of the mosquito gut. We found that QS-activated phenylalanine metabolism directly regulates the biogenesis of outer membrane vesicles (OMVs) that facilitate bacterial biofilm-like aggregation and promote *Serratia* survival and persistence in the gut of blood-fed mosquitoes. These findings suggest promising strategies for blocking *Plasmodium* transmission by *Anopheles* mosquitoes and for containing the spread of malaria.

RESULTS

Symbiotic Su_YN1 colonizes the mosquito gut by forming biofilm-like aggregates

To investigate the mechanism underlying commensal adaptation to the gut of blood-fed mosquitoes, we compared the colonization dynamic of the symbiotic bacterium S. ureilytica Su YN1 with those of an opportunistic non-symbiotic bacterium E. coli DH5α, in Anopheles mosquitoes (Dutch strain) after a blood meal. Su_YN1 efficiently proliferated after a blood meal and stably persisted in the female mosquito midgut, whereas DH5 α poorly colonized the gut and was rarely observed after 36 h following a blood meal (Figures 1A and 1B). We sectioned midguts at 48 h after blood feeding and found that most of the opportunistic DH5 α bacteria were egested, and the few that remained in the gut were loosely distributed (Figure 1C, upper, Giemsa staining). Conversely, abundant Serratia Su_YN1 bacteria populated the mosquito midgut and formed biofilm-like aggregates (Figure 1C, lower, Giemsa staining). Moreover, S. marcescens AS1, another commensal Serratia bacterium that stably colonizes Anopheles mosquitoes, 19 also forms biofilm-like aggregates in the midgut of blood-fed mosquitoes (Figure S1A), suggesting that high-ordered aggregation facilitates commensal Serratia bacteria colonization of the gut.

We next stained mosquito midgut sections using fluorescein isothiocyanate (FITC)-Concanavalin A as a marker of extracellular polymeric substances (EPSs). Su_YN1 aggregates were detected in midguts of blood-fed mosquitoes, indicating the formation of biofilm-like structures (Figure 1C, FITC lane). To directly observe whether Su_YN1 forms bona fide biofilm-like aggregates, we tore open mosquito midguts and searched for Su_YN1 colonies using cryo-scanning electron microscopy (cryo-SEM). We detected large numbers of OMVs within the Su_YN1-produced matrix, resulting in the formation of biofilm-like aggregates that wrap bacteria into patches (Figure 1D).

OMVs are spherical nanostructures secreted by bacteria for the transport of proteins, phospholipids, lipopolysaccharides (LPS), and nucleic acids between cells.²⁴ OMVs can mediate the aggregation of cells and may help promote the development of biofilm structure. 25-27 We cultured Su_YN1 on cover slips and searched for biofilm-like aggregates using transmission electron microscopy (TEM). Abundant OMVs were observed in these bacterial aggregates (Figure S1B). These OMVs within the biofilm-like aggregates on the cover slip showed morphology similar to OMVs from the planktonic culture (Figure S1B). Notably, OMVs seem to adhere to each other after release (Figures S1B and S1C), which may promote aggregation and development of biofilm-like structures. To test whether Su_YN1 OMVs directly promote aggregation, we purified OMVs from a planktonic culture and added these OMVs to the culture of Su_YN1 growing statically on cover slips and found that OMV addition promoted aggregate formation in a dosedependent manner (Figure 1E). The observation of large numbers of OMVs in Su_YN1 aggregates suggests that these blood meal-induced OMVs may play a critical role in driving Su_YN1 aggregate formation and gut colonization.

The AHL QS system mediates Su_YN1 gut colonization via OMV-driven biofilm-like aggregation

The above results indicate that OMV-derived biofilm-like aggregation plays a major role in promoting *Serratia* Su_YN1 bacteria survival in the hostile midgut environment of blood-fed mosquitoes (Figure 1F). Of note, during blood digestion, Su_YN1 profoundly proliferates within 24 h, reaching about 10⁵–10⁷ per midgut (Figure S1D) and forming high-density aggregation clusters in the midgut (Figure S1E).

For most bacterial species, including Pseudomonas aeruginosa and Serratia marcescens, high population density usually activates QS, a process of cell-cell chemical communication via secreted signal molecules that lead to synchronous alteration of behavior responses.²⁸⁻³⁰ To test whether the QS system is involved in gut colonization, we searched the Su_YN1 genome sequence data (NCBI GenBank assembly accession: GCA_017565285.1) for potential QS genes. We found that Su_YN1 harbors a classic N-acyl homoserine lactone (AHL) QS system (Figure 2A). The AHL QS system in Serratia bacteria typically utilizes a Luxl family synthase to generate AHL signal molecules. These are sensed by a LuxR-type transcriptional regulator that usually acts as a gene repressor.31 Our analysis revealed that Su_YN1 harbors an intact AHL-type QS system that comprises a LuxI synthase and a LuxR-type regulator genes arranged in opposite directions (Figure 2A). These are named Suel (gene ID: NPGAP00150) and SueR (gene ID: NPGAP00145), respectively. Comparative protein sequence analysis of SueR showed high sequence similarity with its orthologs from other Serratia bacteria (Figure S2).

We next asked whether the Suel/SueR QS circuit regulates Su_YN1 biofilm-like aggregation. We constructed *Suel*-knockout (KO) and *SueR*-KO QS mutant strains and quantified aggregate biomass using crystal violet staining. Compared with the wild-type (WT) strain, bacterial aggregation was significantly reduced in *Suel*-KO mutant while substantially increased in the *SueR*-KO mutant (Figure 2B). Further observation using confocal microscopy showed that the *SueR*-KO

Article



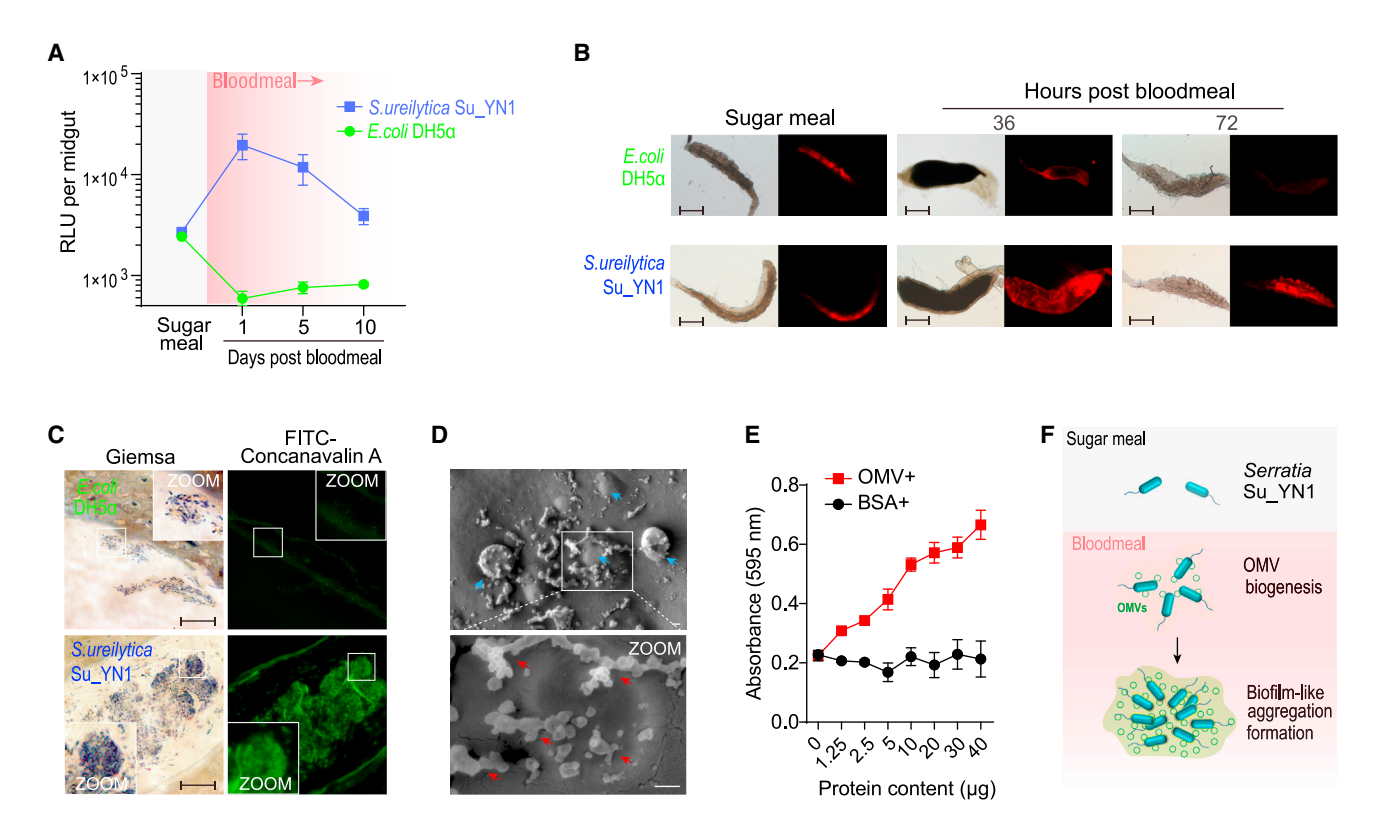


Figure 1. Symbiotic Serratia Su YN1 colonizes mosquito gut by forming biofilm-like aggregates

(A) 10⁷ colony-forming units (CFUs) of Renilla luciferase-expressing Serratia Su_YN1 or E. coli DH5α were fed to A. stephensi mosquitoes, and the relative light unit (RLU) was measured in the midguts at different time points before and after a blood meal. n = 10 in each group.

(B) Red fluorescent protein mScarlet-expressing Serratia Su YN1 or E. coli DH5α were fed to A. stephensi mosquitoes, and midgut bacteria were visualized at different time points before and after a blood meal. Bright-field images (left) are paired with the corresponding fluorescent images (right). Scale bars repre-

(C) A. stephensi mosquitoes carrying Serratia Su_YN1 or E. coli DH5a were fed with blood, and after 48 h, semi-thin sections of midguts were prepared. Giemsa (left) and FITC-Concanavalin A staining (right) were performed on the sections. Scale bars represent 5 µm.

(D) Cryo-scanning electron microscopy image of the A. stephensi midguts carrying Serratia Su_YN1 48 h after a blood meal. Blue arrowheads indicate Su_YN1 bacteria. Red arrowheads indicate outer membrane vesicles (OMVs). Scale bars represent 200 nm.

(E) Different doses of OMV or BSA (control) were added to Serratia Su_YN1 grown in RPMI1640 + 10% fetal bovine serum (FBS) medium and in vitro biofilm biomass was quantified 24 h later using crystal violet staining and measurement of absorbance at 595 nm. n = 3 in each group.

(F) Schematic diagram showing Su_YN1 OMV biogenesis and biofilm-like aggregation after a blood meal.

Data are presented as the mean \pm SEM in (A) and the mean \pm SD in (E).

See also Figure S1.

mutant formed much thicker aggregates than the WT strain, whereas the Suel-KO mutant produced less aggregation than the WT strain (Figure 2C). To further confirm Suel/SueR QS circuit mediating biofilm-like aggregation in the mosquito, we examined aggregation using midgut semi-thin sections. Suel-KO bacteria produced drastically less aggregation, whereas the SueR-KO strain produced more aggregation compared with the WT strain (Figure 2D). Together, these results indicate that Suel positively regulates biofilm-like aggregation, whereas SueR functions as a repressor of biofilm-like aggregation.

To explore whether QS-activated Su_YN1 biofilm-like aggregation facilitates bacterial gut colonization, we introduced different QS mutant strains into Anopheles mosquitoes and measured their colonization ability after a blood meal. We found a positive correlation of gut colonization and aggregate formation among these QS mutant strains (Figure 2E).

We next asked whether the Suel/SueR QS circuit promotes Su_YN1 aggregation and gut colonization via OMV production. Nanoparticle tracking analysis (NTA) showed that the Suel-KO strain generates fewer OMVs, whereas the SueR-KO strain produced substantially more OMVs (Figure 3A). Similar results were obtained by quantifying OMVs using the bicinchoninic acid (BCA) assay (Figure 3B). Moreover, when observing Serratia aggregation under static cultivation, we found that, compared with the WT strain, the OMV biomass of Suel-KO aggregates was significantly reduced, whereas the OMV biomass of SueR-KO aggregates was significantly increased (Figure S3A). These findings were confirmed by TEM observations (Figure S3B). Suel-gene rescue restored OMV production and aggregate formation (Figure 3C). Notably, adding OMVs to Suel-KO culture promoted aggregate formation (Figure 3D) and reversed its gut colonization deficiency (Figure S3C). Collectively, these results indicate



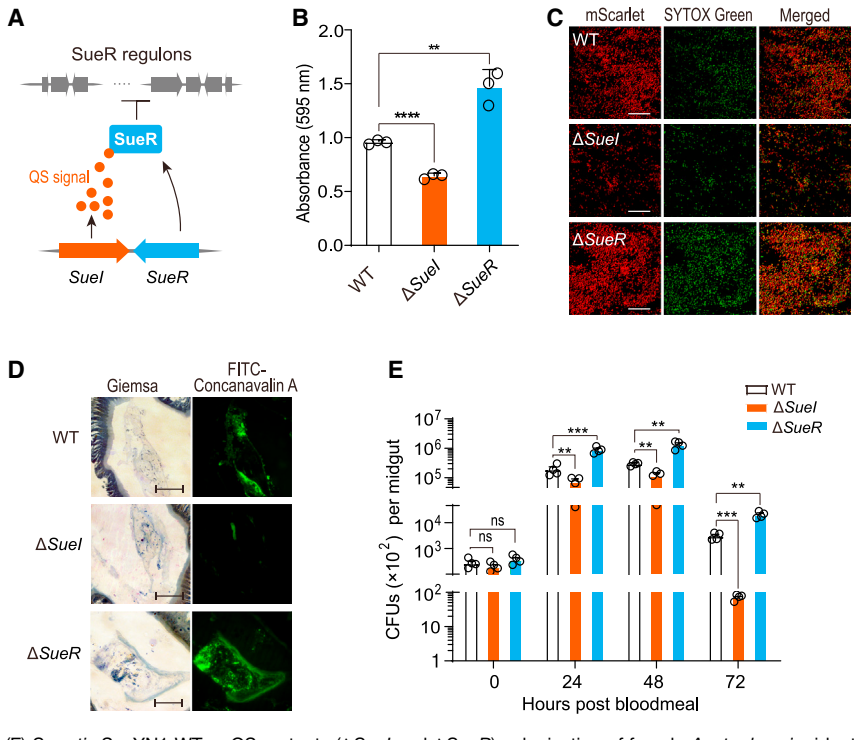


Figure 2. Blood meal activates Serratia Su_YN1 QS that promotes aggregate formation and gut colonization

(A) Schematic representation of the Serratia Su_YN1 AHL-type QS system. The AHL genomic locus encodes a Luxl synthase (Suel) and a LuxR-type regulator (SueR). SueR functions as a repressor of the SueR regulon. The Suel locus produces AHL QS molecules that bind to the SueR repressor and inhibit its function.

(B) Biofilm formation assay of Su_YN1 WT and QS mutant strains using crystal violet staining. Bacteria were grown in RPMI1640 + 10% FBS medium, and biofilm was assayed after 24 h inoculation at 30°C in vitro. n = 3 in each group.

(C) Confocal micrographs of biofilms formed by Serratia Su_YN1 WT strain and QS mutant strains ($\Delta Suel$ and $\Delta Suel$) grown on cover slips for 24 h at 30°C. Living bacteria (as indicated by mScarlet fluorescent protein) and dead bacteria (as indicated by SYTOX Green staining) were visualized. Scale bars represent 5 μ m.

(D) A. stephensi mosquitoes carrying Serratia Su_YN1 WT strain or QS mutant strains (ΔSuel and ΔSueR) were blood fed, and semi-thin sections of midguts were prepared after 36 h. Giemsa staining (left) and FITC-Concanavalin A staining (right) were performed on the semi-thin sections. Scale bars represent 10 μm.

(E) Serratia Su_YN1 WT or QS mutants (Δ SueI and Δ SueI) colonization of female A. stephensi midguts. CFUs were determined in the midguts before and at different times after a blood meal. n = 4 in each group.

Data are presented as the mean \pm SD, and p values were determined by two-tailed unpaired Student's t test in (B) and (E). **p < 0.01; ****p < 0.001; ****p < 0.0001; ns, no significance.

See also Figures S1 and S2.

that the Suel/SueR QS circuit promotes Su_YN1 gut colonization via OMV-driven biofilm-like aggregation.

The C6-HSL QS molecule promotes OMV production and biofilm-like aggregation

QS is a process of bacterial cell-to-cell chemical communication that relies on extracellular chemical signaling molecules called autoinducers. These molecules mediate cell-to-cell chemical communication and allow groups of bacteria to synchronously alter behavior in response to adverse environments via synergistic regulation of gene expression. 32-34 Bacteria of the genus Serratia produce AHL signaling molecules that bind to the SueR receptor to relieve its inhibition of downstream gene expression (Figure 3E). To determine whether Su_YN1 produces specific AHL molecules, we used the CV026 biopigment-based QS biosensor that emits a purple pigment when bacteria produce C4- to C8-AHLs. We found that Suel synthesizes short-chain AHL molecules, that Suel-KO failed to generate AHL molecules, and that Suel-complementation restores AHL production (Figure 3F).

QS can be blocked by quorum-quenching enzymes such as AiiA from *Bacillus* sp., which cleave the lactone ring of the AHLs.³⁶ We introduced a plasmid encoding AiiA into Su_YN1 and confirmed that Su_YN1 OMV production and aggregate formation depend on functional AHL QS molecules (Figure 3G). Su_YN1 *in vivo* colonization capacity was significantly reduced by expressing AiiA (Figure 3G). These results indicate that functional AHL QS molecules play an important role in Su_YN1 gut

colonization. We next used liquid chromatography-tandem mass spectrometry (LC-MS/MS) to identify Su_YN1 AHL QS molecules and found that Su_YN1 produces the AHL signaling molecule C6-HSL (Figure 4A).

We next asked whether C6-HSL directly promotes OMV production and aggregate formation. We added chemically synthesized C6-HSL to a *Suel*-KO culture and found that C6-HSL addition restored OMV production to WT levels (Figure 4B, left). Moreover, C6-HSL addition also restored the biofilm-like aggregation deficiency (Figure 4B, middle) and the colonization deficiency (Figure 4B, right) of the *Suel*-KO strain. Moreover, the addition of chemically synthesized C6-HSL to the WT strain also increased OMV production in a dose-dependent manner (Figure 4C). These results indicate that C6-HSL is a key signal molecule whose synthesis is downstream of Suel and functions to promote OMV production and biofilm-like aggregate formation.

C6-HSL reverses SueR repression of OMV biogenesis and biofilm-like aggregation

We next quantified C6-HSL level in the midgut of *Anopheles* mosquitoes carrying a QS mutant strain. Given that the *Suel* gene is responsible for C6-HSL production, a *Suel*-KO strain produced no detectable C6-HSL molecules in the midgut of mosquito post blood meal, as expected (Figure 4D). *SueR*-KO strain produced substantially more C6-HSL molecules than the WT strain in the midgut of blood-fed mosquitoes (Figure 4D), indicating a possible negative feedback mechanism in the





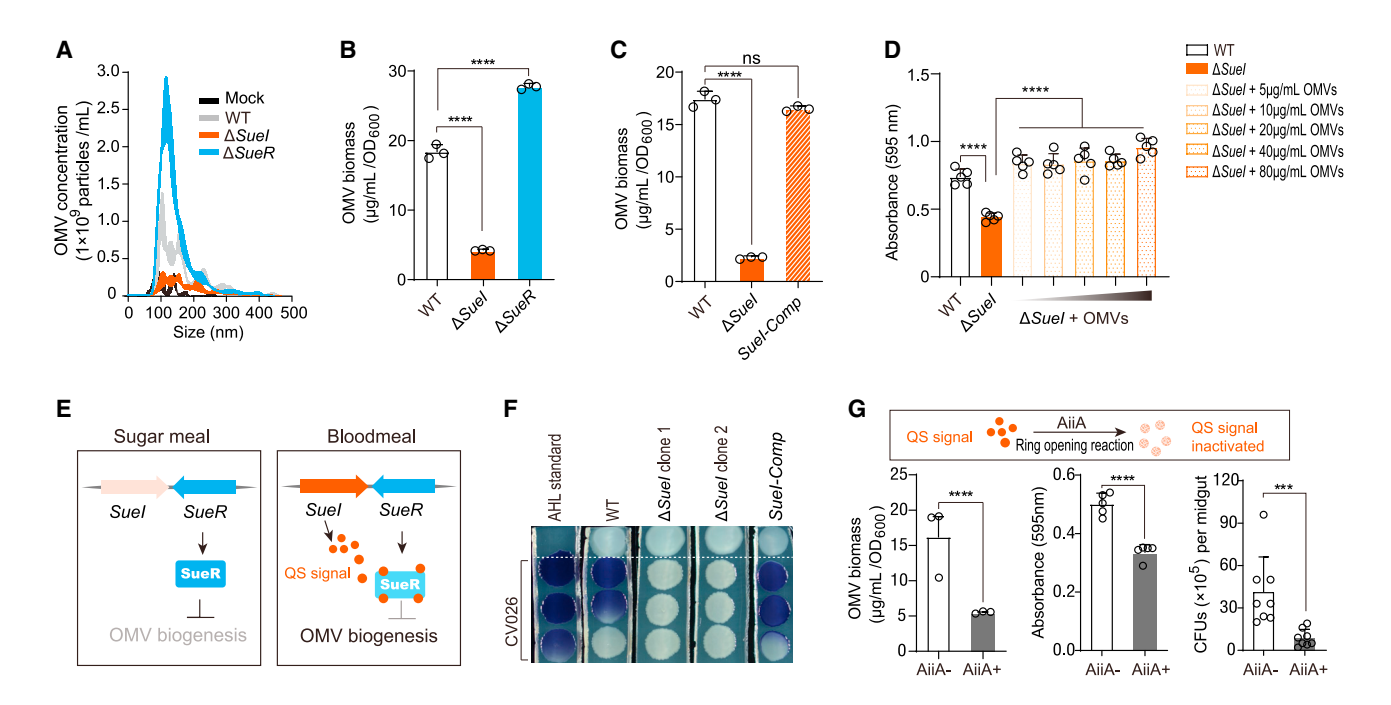


Figure 3. The AHL-type QS system modulates Serratia Su_YN1 gut colonization via OMV-driven aggregate formation

(A) Nanoparticle tracking analysis (NTA) of culture supernatant from Serratia Su_YN1 WT strain and QS mutant strains (ΔSueI and ΔSueI) cultured in RPMI 1640 medium supplemented with extracellular vesicle (EV)-depleted FBS. Blank culture medium containing EV-depleted FBS was used as negative control (Mock). (B) OMV quantification of Serratia Su_YN1 WT strain and QS mutant strains (ΔSuel and ΔSueR) using the bicinchoninic acid (BCA) assay. n = 3 in each group. (C) OMV quantification of Serratia Su_YN1 WT strain, ΔSuel strain, and Suel complemented strain (Suel-comp) using BCA assay. n = 3 in each group. (D) Biofilm formation assay of Serratia Su_YN1 WT, \(\Delta SueI \), and \(\Delta SueI \) strains supplemented with different doses of OMVs using crystal violet staining. n = 5 in

(E) Schematic diagram showing Serratia Su_YN1 QS system status under different conditions. Under sugar meal condition, AHL-type QS is inactive and SueR represses downstream OMV biogenesis pathways. A blood meal activates production of Suel that binds to the SueR repressor, leading to OMV biogenesis. (F) A CV026 reporter system was used as biosensor to detect AHL QS molecules produced by the Serratia Su_YN1 WT strain, the ΔSuel strain, and the Suel complemented strain (Suel-comp). Above the white line is the standard and the sample to be tested, and below the white line is the CV026 strain. A C4-HSL standard was used as a positive control.

(G) Serratia Su_YN1 transformed with empty vector plasmid (AiiA-) or plasmid contains quorum-quenching enzyme AiiA (AiiA+) were tested for OMV biomass (left, n = 3), for in vitro biofilm formation (middle, n = 5), and for gut colonization (right, n = 8).

Data are presented as the mean ± SD, and p values were determined by two-tailed unpaired Student's t test in (B), (C), and (G), one-way ANOVA followed by Tukey's post hoc analysis in (D). ***p < 0.001; ****p < 0.0001; ns, no significance. See also Figure S3.

C6-HSL regulation in the Suel/SueR pathway. Notably, the ability of Suel-KO and SueR-KO strains to produce C6-HSL in the mosquito gut is consistent with the in vitro culture results, indicating that Suel and SueR positively and negatively regulate OMV production and biofilm-like aggregation, respectively. This correlation further confirms that Suel-controlled C6-HSL synthesis induces OMV production that drives biofilm-like aggregation and facilitates Serratia gut colonization.

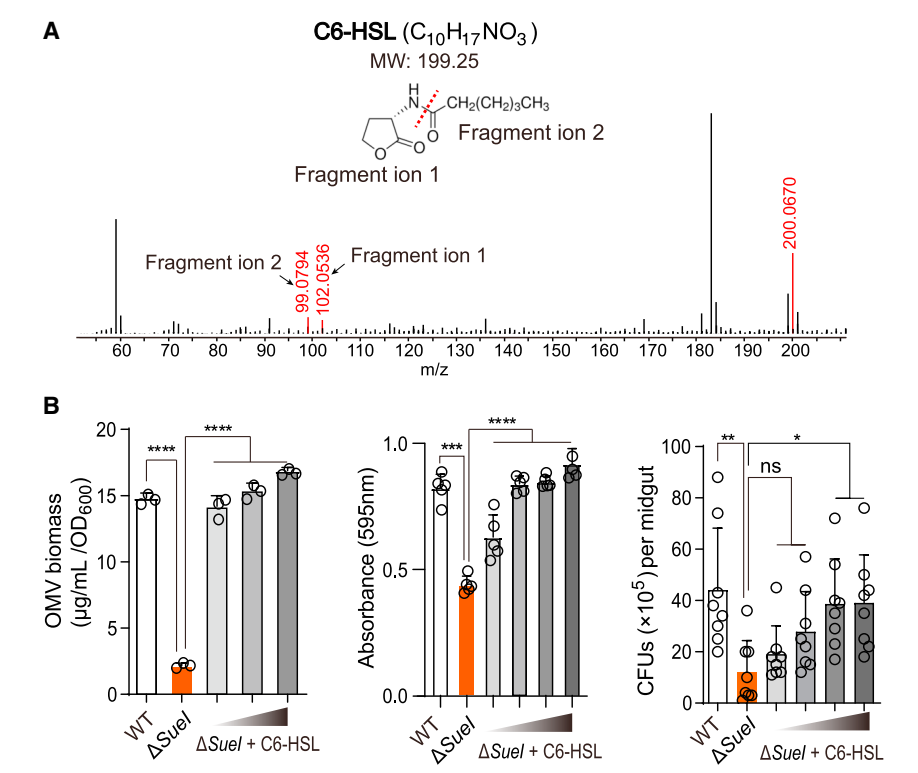
Some specific QS molecules can directly induce OMV formation. Pseudomonas quinolone signal (PQS) molecule of P. aeruginosa, for example, mediates OMV production by asymmetrically inserting into the phospholipid bilayer and causing membrane curvature.37,38 We tested whether C6-HSL can also directly induce membrane curvature using a red blood cell (RBC) detection system. 37 Unlike PQS, C6-HSL failed to induce RBC membrane curvature and hemolysis (Figures S4A and S4B), indicating that C6-HSL drives OMV biogenesis through activation of a downstream signaling pathway, rather than by direct physical action.

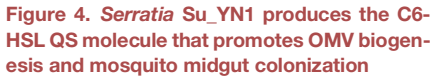
As a non-classical QS system, the Serratia LuxR-type QS receptor is a transcriptional regulator acting as a DNA-binding repressor.39,40 Our data show that the Su_YN1 QS receptor SueR suppresses OMV production and biofilm-like aggregation. We hypothesized that SueR represses OMV biogenesis in the absence of QS signal molecules and that a blood meal activates Suel and production of C6-HSL that binds to SueR to relieve its repression (Figure 3E). Although the underlying mechanisms for driving bacterial OMV biogenesis remain elusive, several genes encoding lipoproteins and outer membrane proteins are involved in OMV biogenesis, including Ipp, ompA, pal, and tolB. 41,42 Using real-time qPCR, we confirmed that these OMV signature genes are inhibited upon Suel deletion and activated upon SueR deletion (Figures S4C-S4F), indicating that C6-HSL accumulation reverses the repression by SueR and initiates OMV production (Figure 5A).

C6-HSL binding to SueR activates a phenylalanine metabolic gene cluster that in turn drives OMV biogenesis

Our observation that the addition of C6-HSL or SueR deletion unleashed the OMV biogenesis pathways (Figure 5A) prompted us to seek the identification, using high-resolution RNA sequencing







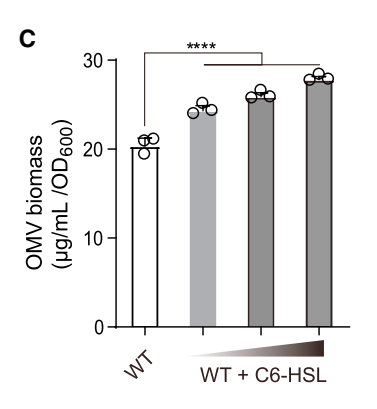
(A) Structure identification of QS signal molecule produced by *Serratia* Su_YN1 using LC-MS/MS analysis. The major fragments of the C6-HSL molecule are indicated with black arrows.

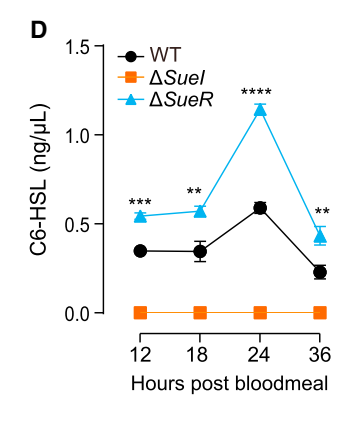
(B) C6-HSL supplementation reverts the $\Delta Suel$ deficiency. Serratia Su_YN1 WT strain, $\Delta Suel$ strain, and Suel strain supplemented with different doses of C6-HSL (left: 10, 20, and 40 nM; middle and right: 5, 10, 20, and 40 nM) were tested for OMV biomass (left, n = 3), for in vitro biofilm formation (middle, n = 5), and for in vivo gut colonization (right, n = 8).

(C) C6-HSL supplementation further improves OMV biogenesis of wild-type Serratia Su_YN1. OMVs from Serratia Su_YN1 WT strain and WT strain supplied with different doses of C6-HSL (10, 20, and 40 nM) were quantified using the BCA assay. n = 3 in each group.

(D) A. stephensi mosquitoes carrying Serratia Su_YN1 WT or QS mutants ($\Delta SueI$ and $\Delta SueR$) were blood fed, and the midguts were dissected at different time points after a blood meal and homogenized for measurement of C6-HSL content using LC-MS/MS analysis. n = 3 in each group.

Data are presented as the mean \pm SD, and p values were determined by one-way ANOVA followed by Tukey's post hoc analysis in (B) and (C), two-tailed unpaired Student's t test in (D). *p < 0.05; **p < 0.01; ***p < 0.001; ****p < 0.0001; ns, no significance.





(RNA-seq) analysis, of the activated pathways involved in QS-driven OMV biogenesis. We compared the transcription profiles of the WT strain (WT) vs. the WT strain treated with C6-HSL (WT + C6-HSL) and of the WT strain (WT) vs. the SueR-KO strain (SueR-KO). The two comparisons exhibited similar activated transcription profiles. Kyoto Encyclopedia of Genes and Genomes (KEGG) functional enrichment analysis showed that several gene clusters, especially genes of the phenylalanine metabolic pathway, were dramatically up-regulated in the C6-HSL-treated WT strain and in the SueR-KO mutant (Figures 5B and S5A). Metabolic pathway analysis disclosed that the up-regulated phenylalanine metabolic gene cluster is responsible for the conversion of phenylalanine to phenylacetyl-coenzyme A (CoA) and acetyl-CoA (Figure S5A).

The phenylalanine metabolic gene cluster shares a common promoter region, which may include the SueR binding site

(Figure S5B). qPCR analysis confirmed that the gene cluster is responsive to Suel/SueR deletion. Compared with the WT strain, the expression levels of genes involved in phenylalanine metabolism were significantly reduced in *Suel-*KO strain, whereas the transcription levels were significantly increased in *SueR-*KO strain (Figure 5C). We conducted electrophoretic mobility shift assays (EMSAs) to investigate whether the phenylalanine metabolic gene cluster is a bona fide SueR regulon under the control of the

Suel/SueR circuit. To perform the assay, we incubated Cy5labeled DNA fragments containing the promoter region of the phenylalanine cluster with purified SueR protein at varying concentrations and measured the binding affinity. The results from EMSA clearly indicate that SueR protein exhibits dose-dependent binding affinity to the DNA probes, resulting in a decrease in mobility (Figure 5D). Furthermore, the proposed model of SueR action suggests that the presence of C6-HSL leads to the inhibition of SueR's DNA-binding capability. To validate this hypothesis, SueR was incubated with varying concentrations of C6-HSL and subjected to EMSA testing. Consistent with our model, the results demonstrate that the ability of SueR to bind DNA was progressively inhibited by C6-HSL in a dose-dependent manner by C6-HSL (Figure 5E). To directly show that C6-HSL activates the phenylalanine metabolic gene cluster via depressing SueR, we created a 293T cell





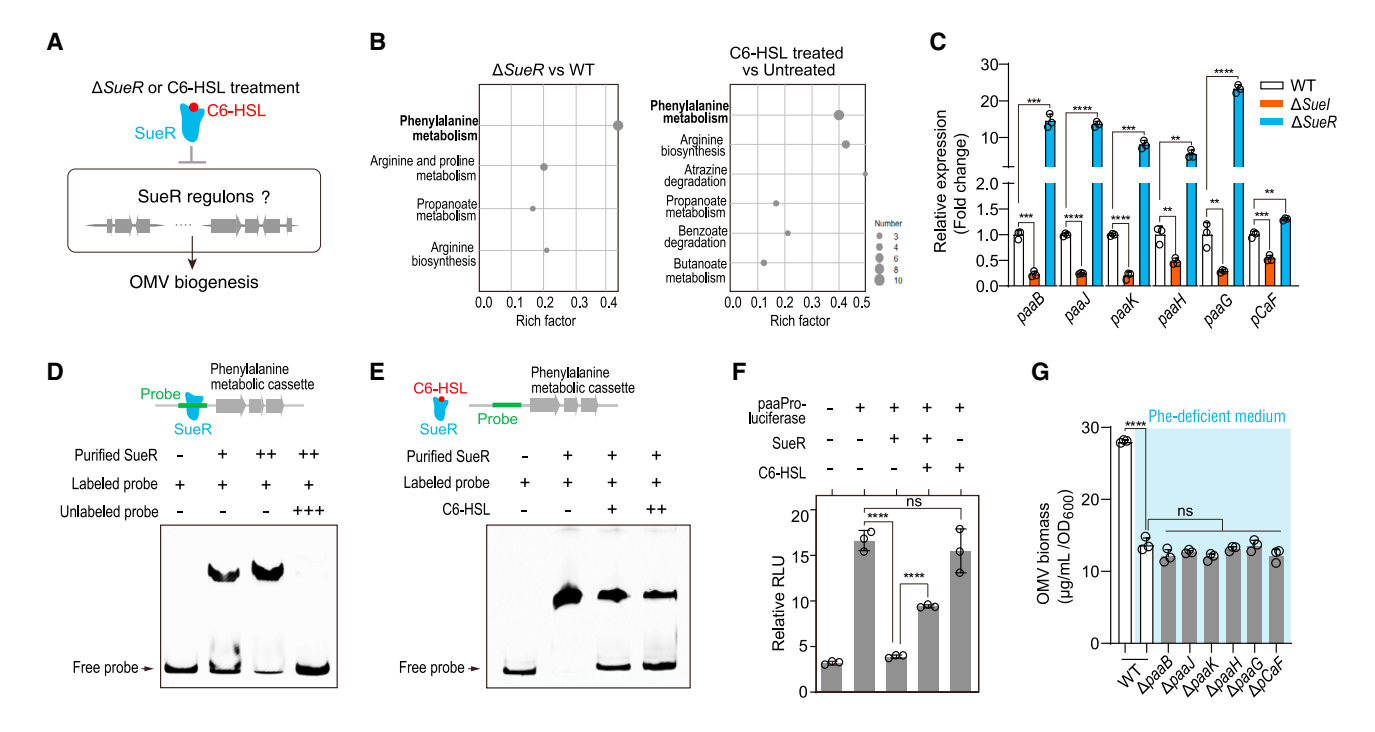


Figure 5. QS activates the phenylalanine metabolic pathway to promote OMV biogenesis

(A) Schematic diagram of the QS-regulated OMV biogenesis pathway.

(B) KEGG enrichment annotation of the comparative transcriptome between Serratia Su_YN1 WT strain and ΔSueR mutant strain (left), and between C6-HSLtreated and untreated Su_YN1 WT strain (right). Significant upward adjustments are marked with gray dots.

(C) qPCR analysis of the expression level of phenylalanine metabolism genes by Serratia Su_YN1 WT strain and quorum-sensing mutant strains (\(\Delta Sue \) and $\Delta SueR$). The 16S rRNA gene was used as reference. n = 3 in each group.

(D) Electrophoretic mobility shift assay (EMSA) showing the association of SueR with the promoter region of phenylalanine metabolism gene cluster. Cy5-labeled DNA fragments containing the promoter regions of the phenylalanine cluster were used as probes. Increasing concentration (20 and 40 nM) of purified small ubiquitin-like modifier(SUMO) tag SueR protein was incubated with DNA probe (100 nM) or unlabeled probe (1,000 nM) and tested in EMSA.

(E) C6-HSL binding to SueR relieves its affinity and repression on the promoter region of phenylalanine metabolism gene cluster. Increasing concentrations (40 and 80 nM) of C6-HSL were incubated with SueR (40 nM) and DNA probe (100 nM) and tested in EMSA.

(F) Dual-luciferase reporter assay for detection of the interaction between SueR and the promoter of phenylalanine metabolism gene cluster. Plasmids expressing SueR and promoter region of the phenylalanine metabolism gene cluster were co-transfected into HEK293T cells and then treated with or without C6-HSL (40 nM). Relative expression of the phenylalanine metabolism gene cluster driving luciferase was determined by measuring RLU, n = 3 in each group.

(G) OMV quantification of Serratia Su_YN1 WT strain and phenylalanine gene mutant strains (ΔρααΒ, ΔρααΑ, Δ RPMI 1640 medium or phenylalanine-deficient RPMI 1640 medium (Phe-deficient medium). n = 3 in each group.

Data are presented as the mean ± SD, and p values were determined by two-tailed unpaired Student's t test in (C) and (F), one-way ANOVA followed by Tukey's post hoc analysis in (G). **p < 0.01; ***p < 0.001; ****p < 0.0001; ns, no significance. See also Figures S4 and S5.

reporter system, placing the luciferase gene under the control of the phenylalanine cluster promoter region (Figure S5B). Co-expression of SueR in the reporter cell caused a significant decrease in the luciferase signal. However, the addition of C6-HSL reversed this inhibition (Figure 5F). These findings suggest that SueR plays a direct role in repressing the phenylalanine cluster and that C6-HSL can effectively reverse this repression.

We next examined the association between phenylalanine metabolism and Su_YN1 OMV production by constructing phenylalanine metabolism mutant strains (paaB-KO, paaJ-KO, paaK-KO, paaH-KO, paaG-KO, and pCaF-KO) (Figure S5B). These mutant strains grew normally (Figure S5C), but all showed reduced OMV production (Figure S5D) and biofilm-like aggregation (Figure S5E). To further corroborate the involvement of phenylalanine metabolism in OMV biogenesis, we set up a phenylalanine-deficient RPMI 1640 medium (Phe-deficient medium) and cultured the mutant strains in this medium. Compared with non-deficient medium, the OMV production and biofilm-like aggregation of the WT strain were significantly reduced in the Phe-deficient medium, to a level comparable to that of phenylalanine metabolic gene-deletion strains (Figure 5G). These results suggest that Serratia Su_YN1 OMV production is mediated by phenylalanine metabolism.

Metabolic conversion of phenylalanine to acetyl-CoA drives OMV biogenesis

Biogenesis of OMVs requires robust lipid metabolism and substantial ATP consumption. 43-45 Acetyl-CoA, in particular, is a pivotal intermediate for fatty acid chain elongation that drives lipid synthetic metabolism. 46,47 Acetyl-CoA also directly feeds into the tricarboxylic acid (TCA) cycle to generate ATP, which is also important for lipid synthetic metabolism. C6-HSL (or SueR deletion)-mediated activation of the phenylalanine



Cell Host & Microbe Article

metabolic pathway may lead to elevated acetyl-CoA and ATP pools, which in turn drive OMV biogenesis (Figure 6A).

Next, we asked whether phenylalanine is metabolically converted into acetyl-CoA and ATP during OMV biogenesis. We found that both acetyl-CoA (Figure 6B) and ATP production (Figure S6A) were significantly reduced in phenylalanine metabolism mutant strains. Furthermore, we found that the acetyl-CoA (Figure 6C) and ATP levels (Figure S6B) of the Suel-KO strain were significantly reduced. The reduction could be reversed by C6-HSL supplementation, and acetyl-CoA and ATP production of SueR-KO bacteria was increased (Figures 6C and S6B). In addition, acetyl-CoA and ATP levels were reduced when bacteria were cultured in Phe-deficient medium, whereas phenylalanine supplementation significantly increased acetyl-CoA and ATP production (Figures 6D and S6C).

To rule out the possibility that the C6-HSL-stimulated acetyl-CoA pool elevation results from pathways other than the phenylalanine metabolic pathway, we carried out isotope tracing experiments using ¹³C-labeled phenylalanine. Su_YN1 was cultured in Phe-deficient medium supplemented with ¹³C-labeled phenylalanine. As expected, the isotope-labeled acetyl-CoA derived from ¹³C-labeled phenylalanine could be readily detected (Figure S6D). In addition, disruption of the phenylalanine metabolic gene cluster strongly inhibited the conversion of ¹³C-labeled phenylalanine to acetyl-CoA (Figure 6E).

We next asked whether the metabolic conversion of phenylalanine into acetyl-CoA, or further biotransformation of acetyl-CoA, actually promotes OMV biogenesis. We used an acetyl-CoA synthase inhibitor (inhibitor 1) to partially inhibit the formation of acetyl-CoA. We also used olumacostat glasaretil (inhibitor 2), an acetyl-CoA carboxylase inhibitor that inhibits the biotransformation of acetyl-CoA via the type II fatty acid synthesis (FASII) pathway. Adding inhibitor 1 or inhibitor 2 at low concentration (2 μ M) to the Su_YN1 culture significantly inhibited OMV production, even under the stimulation by C6-HSL (Figure 6F). However, we did not observe an obvious impact on bacterial growth. Taken together, these data reveal a fundamental metabolic mechanism by which C6-HSL-regulated QS phenylalanine metabolic pathway leads to the acetyl-CoA- and ATP-dependent OMV biogenesis.

C6-HSL enhances Serratia gut colonization and enhances mosquito refractoriness to Plasmodium

Serratia Su_YN1 strongly inhibits the development of malaria parasites when it colonizes the mosquito gut and can naturally and rapidly spread through mosquito populations. 17 To this end, we further examined the anti-Plasmodium effectiveness of the QS mutant bacteria. The mutant strains were introduced into Anopheles mosquitoes followed by feeding Plasmodium infectious blood. We used the human P. falciparum NF54W and P. berghei ANKA 2.34 to infect A. stephensi in the following assays. Compared with the WT strain, the Suel-KO mutant strain showed a significant reduction in Plasmodium-killing activity, whereas the SueR-KO mutant strain showed more potent activity against both human (Figure 7A, left) and rodent Plasmodium parasites (Figure S7A). Moreover, Su_YN1 bacteria expressing a quorum-quenching enzyme strongly reduced anti-Plasmodium activity (Figures 7A, right, and S7B). Moreover, we found that the more Serratia Su_YN1 colonizes the mosquito gut, the higher antimalarial lipase (AmLip) it produces (Figures S7C and S7D). Thus, the anti-*Plasmodium* activity of gut bacteria was positively correlated with their gut colonization ability, indicating that improving gut colonization of antimalarial symbionts will lead to enhanced *Plasmodium*-transmission blocking activity.

As C6-HSL is a potent QS signaling molecule promoting *Serratia* gut colonization, we hypothesized that exposing mosquitoes to C6-HSL will improve *Serratia* gut adaptation and increase its abundance. Exposure of *Anopheles* mosquitoes to C6-HSL for 30 min (Figure 7B), led to more *Serratia* spp. bacteria in the midgut (Figure 7C). Moreover, compared with controls, exposing mosquitoes to C6-HSL significantly enhanced Su_YN1 gut colonization (Figure 7D) and reduced the *Plasmodium* burden in a dose-dependent manner (Figure 7E). Thus, exposing mosquitoes to C6-HSL provides a promising strategy for enhancing commensal gut colonization and mosquito resistance against *Plasmodium* infection.

DISCUSSION

Bacteria rely on synergistic community behavior and high-ordered aggregate structure formation to cope with hostile environment, and QS is fundamental to our understanding of how bacteria cells communicate and behave as a community. Emerging evidence suggests that QS may also promote bacterial adaptation to the host gut.⁵¹ However, much of our current knowledge of QS-mediated adaptation comes from research on pathogenic bacteria using in vitro systems, while our understanding of bacteria QS within the host is still lacking. Although the involvement of QS is recognized as critical for bacterial adaptation to the harsh gut microenvironment, the metabolic context remains ambiguous. In this study, we report that an AHL QS system is required for symbiotic Serratia bacteria to colonize the mosquito gut and uncovered a phenylalanine metabolic cascade that regulates the biogenesis of OMVs, which facilitate bacterial biofilm-like aggregation and promote Serratia colonization of the hostile gut environment of blood-fed mosquitoes. Our findings provide the first clear evidence that the SueR QS receptor directly represses a phenylalanine cassette, whereas C6-HSL binding to SueR relieves the repression. We identified the phenylalanine cassette as a direct QS target, revealing a critical crosstalk between QS and amino acid metabolism.

Gut commensals have to adapt and survive the harsh gut microenvironment. Unlike many pathogenic bacteria that typically form surface-attached biofilms, gut commensals are usually separated from the gut epithelial cell by physical barriers such as the mucus layer in mammals and the chitinous peritrophic matrix (PM) in insects. Gut microbiota needs to survive the hostile gut lumen of blood-fed mosquitoes, where blood digestion turns the gut into a stressful environment due to high oxidative stress. Our study indicates that QS activation enables Serratia Su_YN1 to form biofilm-like aggregates in the blood bolus. Normally, biofilms develop on a substratum during unfavorable conditions and are immersed in a polymeric matrix secreted by the bacteria.⁵² Biofilms are usually formed by resting,53 rather than by rapidly proliferating bacterial communities such as the Serratia Su_YN1 reported here. Similar aggregate structures were also observed in other mosquito commensals like Pantoea,⁵⁴ but have not been further investigated.





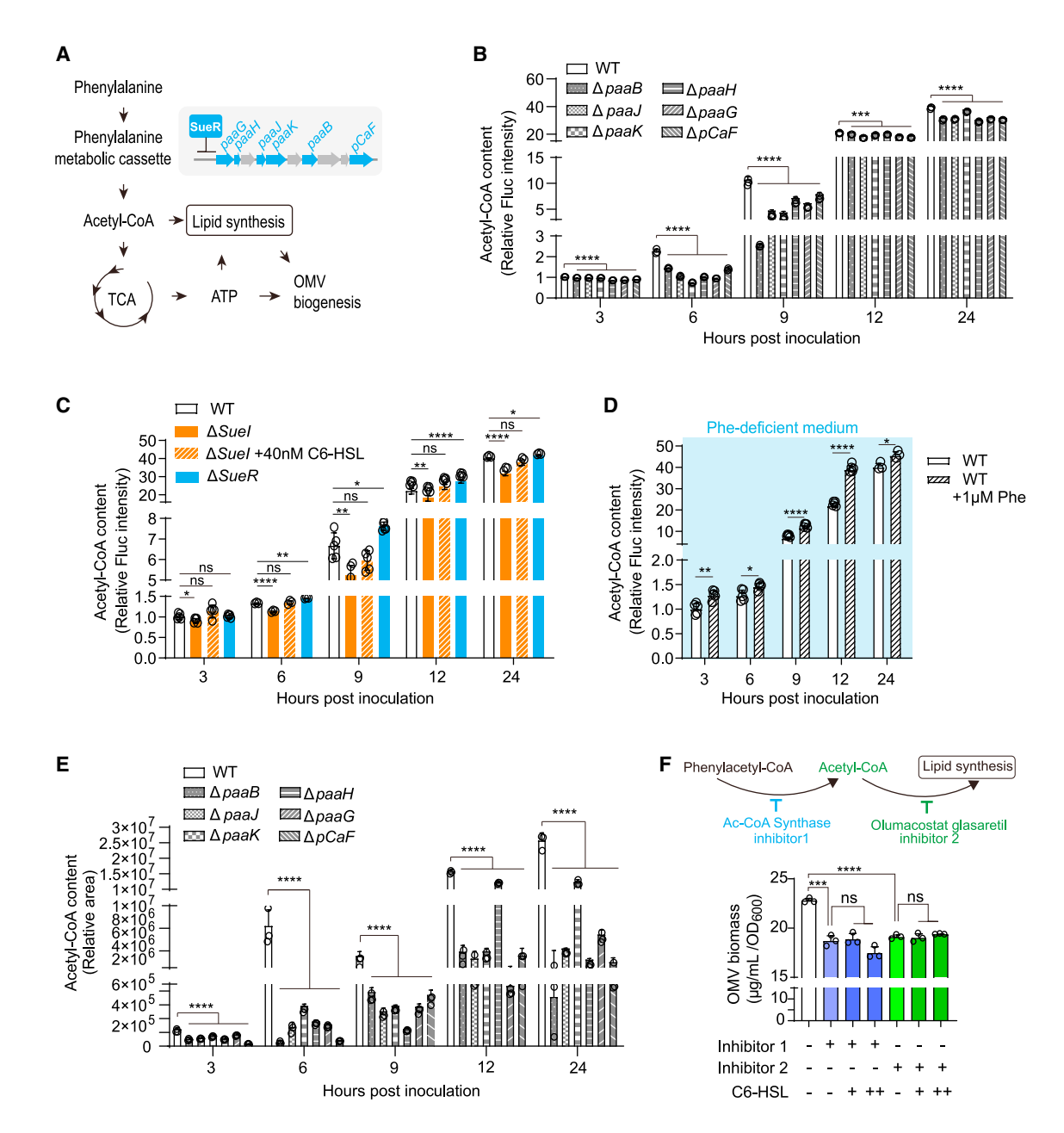


Figure 6. The metabolic conversion of phenylalanine to acetyl-CoA drives OMV biogenesis

(A) Schematic diagram of OMV biogenesis promoted by C6-HSL-activated phenylalanine metabolic pathway.

- (B) Time course of bacterial acetyl-CoA content of Serratia Su_YN1 WT and phenylalanine gene mutant strains (ΔρααΒ, ΔρααΒ, ΔρααΚ, ΔρααΗ, ΔρααΘ, and $\Delta pCaF$). n = 3 in each group.
- (C) Time course of bacterial acetyl-CoA content of Serratia Su_YN1 WT strain, of QS mutant strains (\(\Delta Sue I\) and \(\Delta Sue R \)), and of the \(\Delta Sue I\) mutant strain supplied with C6-HSL. n = 3 to 5 in each group.
- (D) Bacterial acetyl-CoA content quantification of Serratia Su_YN1 WT strain cultured in phenylalanine-deficient medium, supplied or not with 1 µM phenylalanine. n = 5 in each group.
- (E) Isotope tracing of bacterial ¹³C-labeled acetyl-CoA of Serratia Su_YN1 WT strain and phenylalanine gene mutant strains (ΔρααΒ, ΔρααΙ, Δ $\Delta paaG$, and $\Delta pCaF$) cultured in phenylalanine-deficient medium supplied with ¹³C labeled phenylalanine. n = 3 in each group.
- (F) OMV quantification of Serratia Su_YN1 bacteria treated with either an acetyl-CoA synthase inhibitor (inhibitor 1, 2 µM) or olumacostat glasaretil (inhibitor 2, 2 µM), at the concentration that had no obvious impact on bacterial growth, together with C6-HSL (20 or 40 nM). Su_YN1 bacteria treated with DMSO was used as the control. n = 3 in each group.

Data are presented as the mean ± SD, and p values were determined by one-way ANOVA followed by Tukey's post hoc analysis in (B), (C), (E), and (F), two-tailed unpaired Student's t test in (D). *p < 0.05; **p < 0.01; ****p < 0.001; ****p < 0.0001; ns, no significance. See also Figure S6.



Cell Host & Microbe Article

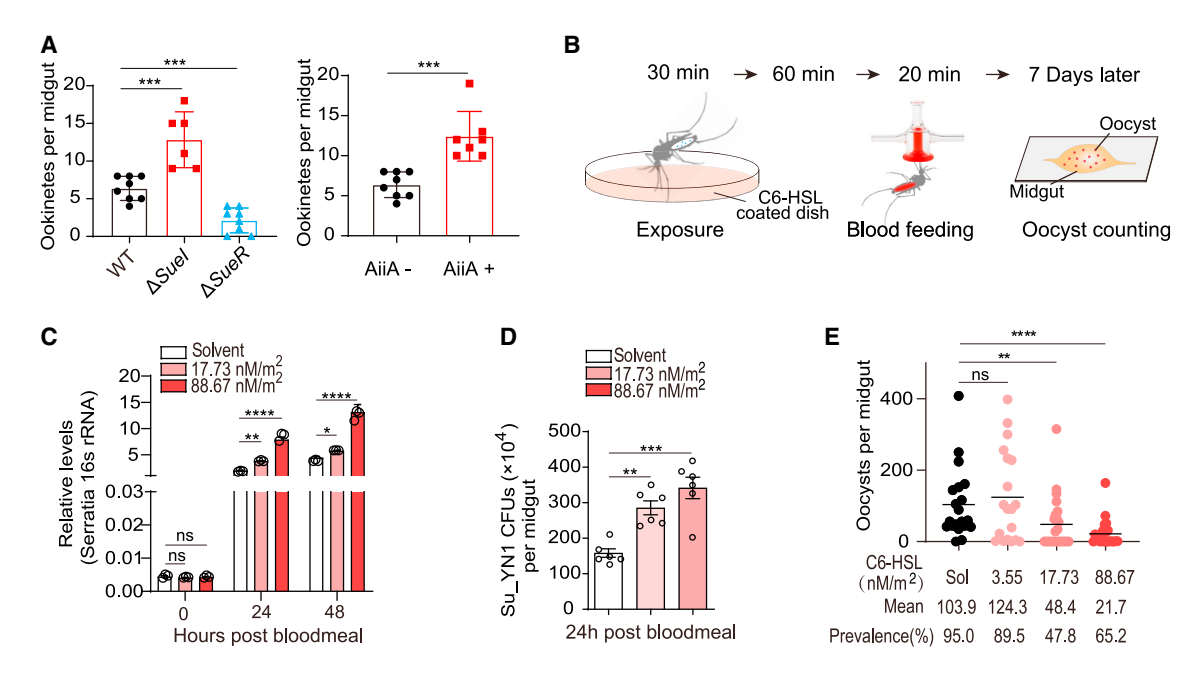


Figure 7. C6-HSL improves Serratia Su_YN1 gut colonization and enhances mosquito refractoriness to Plasmodium infection

(A) P. falciparum NF54W ookinete load of A. stephensi mosquitoes carrying Serratia Su_YN1 WT strain or QS mutant strains ($\Delta Suel$ and $\Delta SueR$) (left), and ookinete load of A. stephensi mosquitoes carrying Serratia Su_YN1 transformed with empty vector plasmid (AiiA-) or plasmid encoding the quorum-quenching enzyme AiiA (AiiA+) (right). n = 6-8 in each group.

(B) Schematic diagram of the experiment that exposes *A. stephensi* mosquitoes to a dish coated with C6-HSL prior to blood feeding on a membrane feeder. (C) *A. stephensi* mosquitoes carrying *Serratia* Su_YN1 were treated with various concentrations of C6-HSL for 30 min as illustrated in (B). *Serratia* bacteria numbers were quantified by qPCR at different time points. n = 3 in each group.

(D) A. stephensi mosquitoes carrying Serratia Su_YN1 were treated with various concentrations of C6-HSL for 30 min as illustrated in (B), before blood feeding. Midguts were dissected 24 h post blood meal, and Su_YN1 CFUs were determined. n = 6 in each group.

(E) Serratia Su_YN1-carrying A. stephensi mosquitoes treated with various concentrations of C6-HSL for 30 min as illustrated in (B), before feeding on Pb ANKA infectious blood. Midgut oocyst numbers were determined 7 days after feeding. The dots represent number of oocysts in individual midguts, and the horizontal lines indicate the mean (n = 20-24). The infection prevalence (infection rate) and infection intensity (mean) were provided.

Data are presented as the mean \pm SD in (A), (C), and (D), mean in (E). p values were determined by two-tailed Mann-Whitney test in (A) and (E), two-tailed unpaired Student's t test in (B) and (C). *p < 0.05; **p < 0.01; ***p < 0.001; ****p < 0.0001; ns, no significance. See also Figure S7.

Biofilm-like aggregates are also found under hydrodynamic conditions, such as vortical flow, ⁵⁵ and show high heterogeneity of biofilm structures. ⁵³ Our findings suggest that gut commensals may also form high-ordered biofilm-like aggregates in other hematophagous insects and animal gut for adaptation to the hostile gut microenvironment.

The biofilm-like aggregates of Serratia that we observed are driven by OMV formation. OMVs are bacterial nanoparticles that contain molecules involved in cell-cell communication. OMVs play important roles in bacterial pathogenesis, intercellular interactions, and adaptation to environments.44 Although OMV biogenesis has been observed in various bacteria, the underlying mechanism and driving force remain largely obscure. Current models propose that OMV biogenesis involves dysregulation of cell wall or outer membrane remodeling, 45,56,57 but a metabolic mechanism for OMV formation is still lacking. In this study, we identified an AHL-activated phenylalanine metabolic cascade that is involved in OMV biogenesis. This metabolic pathway converts phenylalanine to acetyl-CoA, a key metabolic intermediate with diverse physiological functions. OMV biogenesis requires a substantial energy supply and robust lipid biosynthesis. We demonstrate that an elevated acetyl-CoA pool readily

feeds into the TCA cycle to generate ATP, providing energy for OMV production. Acetyl-CoA also serves as a primer for *de novo* synthesis of long-chain fatty acids that can serve as biosynthetic precursors of the OMV-associated lipids. Although we are still unclear how acetyl-CoA is further transformed into building blocks for OMV biogenesis, our findings suggest that amino acid metabolism-directed metabolic flow plays a crucial role in OMV biogenesis by providing the necessary energy. The metabolic conversion and accumulation of key metabolic intermediate, such as acetyl-CoA, may reflect a fundamental mechanism shared by living cells to produce vesicles under stressful conditions.

The significant burden of malaria in developing countries necessitates the urgent development of new approaches to combat this deadly disease. The mosquito midgut constitutes a bottleneck of *Plasmodium* infection of the mosquito. Mosquitoes harbor a highly diverse and dynamic microbiome that profoundly affects host physiology and influences vector competence for human pathogens. One promising strategy for halting *Plasmodium* development is to populate mosquitoes with anti-*Plasmodium* bacteria. However, effective colonization of anti-*Plasmodium* bacteria in the mosquito gut in large numbers

Article



is crucial for the successful implementation of this strategy. 17,19 Unfortunately, most gut bacteria fail to stably colonize the midgut of blood-fed mosquitoes. Moreover, one major obstacle of translating this technique to the field is that the gut microbiota of field mosquitoes is highly complex, which may pose strong competition for the establishment of newly introduced bacteria. Our study demonstrates the potential of using QS molecules to manipulate bacterial symbiosis and enhance colonization resistance against Plasmodium infection. We found that exposing mosquitoes to C6-HSL, an environmentally friendly molecule, promotes the gut colonization of the Plasmodium-blocking Serratia bacterium while improving its Plasmodium transmissionblocking efficacy. These findings suggest that QS molecules may be applied to bed nets or indoor residual spraying to enhance the colonization of anti-parasitic gut bacteria in mosquitoes, providing a promising avenue for improving symbiontbased vector-borne disease control strategies.

Limitations of the study

In this study, we demonstrate that exposing Anopheles mosquitoes carrying Serratia Su_YN1- to C6-HSL QS signal molecule increases Serratia gut colonization and enhances Plasmodium transmission-blocking efficacy, indicating the potential utility of QS molecules in manipulating bacterial symbiosis to bolster resistance against Plasmodium infection. However, more work lies ahead before translating this approach into practical field application. Considering the complex composition of the microbiota in field mosquito populations, conducting additional field studies under ecologically relevant conditions is imperative. Such studies are crucial to comprehensively evaluate Serratia Su_YN1's ability for colonization and spread throughout mosquito populations. Furthermore, these investigations can assess the potential of QS molecules in enhancing symbiont-mediated control of malaria transmission, particularly in the presence of competing bacteria.

STAR*METHODS

Detailed methods are provided in the online version of this paper and include the following:

- KEY RESOURCES TABLE
- RESOURCE AVAILABILITY
 - Lead contact
 - Materials availability
 - Data and code availability
- EXPERIMENTAL MODEL AND STUDY PARTICIPANT **DETAILS**
 - Mouse models and ethics statement
 - Human blood
 - Mosquito model and rearing conditions
 - Bacteria strains and growth conditions
 - O Plasmodium strains and mosquito infection
 - O Mammalian cell culture
- METHOD DETAILS
 - O Colonization and quantification of bacteria in the mosquito midgut
 - O Generation of gene disruption, gene complementation, and quorum quenching enzyme expression strains

- Evolutionary relationship of Serratia SueR proteins
- In vitro biofilm assays
- In vivo biofilm assays
- o mRNA sequencing and data analysis
- CV026 biosensor assay
- O Qualitative and quantitative determination of AHL production by liquid chromatography and mass spectrometry (LC-MS/MS)
- O Bacterial culture for OMV preparation
- O Bacterial RNA extraction
- O Quantitative real-time PCR analysis
- OMV quantification analysis
- O Transmission electron microscopy (TEM) analysis
- O Expression and purification of SUMO-SueR
- O Protein extraction and western blot analysis
- Electrophoretic mobility shift assays (EMSAs)
- Luciferase reporter assays
- Acetyl-CoA and ATP measurement
- [¹³C] Acetyl-CoA measurement
- O Human blood and P. falciparum gametocyte culture
- *In vivo* anti-ookinete formation assay of *P. falciparum*
- O Effect of bacteria on P. berghei infection in mosquitoes
- O Exposing C6-HSL to mosquitoes for P. berghei transmission-blocking assay
- QUANTIFICATION AND STATISTICAL ANALYSIS

SUPPLEMENTAL INFORMATION

Supplemental information can be found online at https://doi.org/10.1016/j. chom.2023.08.017.

ACKNOWLEDGMENTS

This work was supported by grants from the National Natural Science Foundation of China (grants 31830086, 32021001, 32230015, and 32000348), the NSFC/BMGF joint Grand Challenges programs (82261128007 and 2022YFML1006), the National Key R&D Program of China (grant 2019YFC1200800), the Chinese Academy of Science (317GJHZ2022028GC), and the Youth Innovation Promotion Association CAS. We would like to thank Marcelo Jacobs-Lorena at the Johns Hopkins University School of Public Health and Yawen He at Shanghai Jiaotong University for their comments on the manuscript. We are grateful to Fang Li for mosquito rearing. We thank Xiaoyan Xu and Yining Liu from the Core Facility Center of CAS Center for Excellence in Molecular Plant Sciences for their help with LC-MS/MS analysis; Xiaoyan Gao, Jiqin Li, Zhiping Zhang, and Lina Xu for their technical support with electron microscopy; and Wenjuan Cai for the technical support with confocal microscopy. We are grateful to the Malvern Panalytical Company for assisting with nanoparticle tracking analysis.

AUTHOR CONTRIBUTIONS

S.W. conceived the project. S.W., Y.J., and H.G. designed the study. Y.J. performed the majority of the experiments. Y.J. and H.G. performed the OMV quantification analysis. Y.J., L.W., and W.H. performed OMV or EMSA assays. Y.J. and G.W. constructed deletion mutants. Y.J., H.G., and S.W. analyzed data. Y.J., H.G., and S.W. wrote the manuscript.

DECLARATION OF INTERESTS

The authors declare no competing interests.

INCLUSION AND DIVERSITY

We support inclusive, diverse, and equitable conduct of research.



Received: June 2, 2023 Revised: July 24, 2023 Accepted: August 27, 2023 Published: September 21, 2023

REFERENCES

- Barillas-Mury, C., Ribeiro, J.M.C., and Valenzuela, J.G. (2022). Understanding pathogen survival and transmission by arthropod vectors to prevent human disease. Science 377, eabc2757. https://doi.org/10. 1126/science.abc2757.
- Mathilde, G., and George, K.C. (2013). The Anopheles mosquito microbiota and their impact on pathogen transmission. Chapter 17. In Anopheles mosquitoes, M. Sylvie, ed. (IntechOpen). https://doi.org/10. 5772/55107.
- Hand, T.W. (2016). The role of the microbiota in shaping infectious immunity. Trends Immunol. 37, 647–658. https://doi.org/10.1016/j.it.2016. 08.007.
- Leshem, A., Liwinski, T., and Elinav, E. (2020). Immune-microbiota interplay and colonization resistance in infection. Mol. Cell 78, 597–613. https://doi.org/10.1016/j.molcel.2020.03.001.
- Ventura, M., Turroni, F., Motherway, M.O., MacSharry, J., and van Sinderen, D. (2012). Host-microbe interactions that facilitate gut colonization by commensal bifidobacteria. Trends Microbiol. 20, 467–476. https:// doi.org/10.1016/j.tim.2012.07.002.
- Champion, C.J., and Xu, J. (2017). The impact of metagenomic interplay on the mosquito redox homeostasis. Free Radic. Biol. Med. 105, 79–85. https://doi.org/10.1016/j.freeradbiomed.2016.11.031.
- Dworkin, J., and Losick, R. (2001). Linking nutritional status to gene activation and development. Genes Dev. 15, 1051–1054. https://doi.org/10.1101/gad.892801.
- Gao, H., Cui, C., Wang, L., Jacobs-Lorena, M., and Wang, S. (2020).
 Mosquito microbiota and implications for disease control. Trends Parasitol. 36, 98–111. https://doi.org/10.1016/j.pt.2019.12.001.
- Castro-Córdova, P., Mora-Uribe, P., Reyes-Ramírez, R., Cofré-Araneda, G., Orozco-Aguilar, J., Brito-Silva, C., Mendoza-León, M.J., Kuehne, S.A., Minton, N.P., Pizarro-Guajardo, M., et al. (2021). Entry of spores into intestinal epithelial cells contributes to recurrence of *Clostridioides* difficile infection. Nat. Commun. 12, 1140. https://doi.org/10.1038/ s41467-021-21355-5.
- Colangeli, R., Gupta, A., Vinhas, S.A., Chippada Venkata, U.D., Kim, S., Grady, C., Jones-López, E.C., Soteropoulos, P., Palaci, M., Marques-Rodrigues, P., et al. (2020). *Mycobacterium tuberculosis* progresses through two phases of latent infection in humans. Nat. Commun. 11, 4870. https://doi.org/10.1038/s41467-020-18699-9.
- Cansado-Utrilla, C., Zhao, S.Y., McCall, P.J., Coon, K.L., and Hughes, G.L. (2021). The microbiome and mosquito vectorial capacity: rich potential for discovery and translation. Microbiome 9, 111. https://doi.org/10. 1186/s40168-021-01073-2.
- Cirimotich, C.M., Dong, Y., Clayton, A.M., Sandiford, S.L., Souza-Neto, J.A., Mulenga, M., and Dimopoulos, G. (2011). Natural microbe-mediated refractoriness to *Plasmodium* infection in *Anopheles gambiae*. Science 332, 855–858. https://doi.org/10.1126/science.1201618.
- Kajla, M.K. (2020). Symbiotic bacteria as potential agents for mosquito control. Trends Parasitol. 36, 4–7. https://doi.org/10.1016/j.pt.2019. 07.003
- Sassera, D., Epis, S., Pajoro, M., and Bandi, C. (2013). Microbial symbiosis and the control of vector-borne pathogens in tsetse flies, human lice, and triatomine bugs. Pathog. Glob. Health 107, 285–292. https://doi.org/10. 1179/2047773213Y 0000000109
- Wang, Y., Gilbreath, T.M., 3rd, Kukutla, P., Yan, G., and Xu, J. (2011).
 Dynamic gut microbiome across life history of the malaria mosquito Anopheles gambiae in Kenya. PLoS One 6, e24767. https://doi.org/10. 1371/journal.pone.0024767.

- Nouzova, M., Clifton, M.E., and Noriega, F.G. (2019). Mosquito adaptations to hematophagia impact pathogen transmission. Curr. Opin. Insect Sci. 34, 21–26. https://doi.org/10.1016/j.cois.2019.02.002.
- Gao, H., Bai, L., Jiang, Y., Huang, W., Wang, L., Li, S., Zhu, G., Wang, D., Huang, Z., Li, X., et al. (2021). A natural symbiotic bacterium drives mosquito refractoriness to *Plasmodium* infection via secretion of an antimalarial lipase. Nat. Microbiol. 6, 806–817. https://doi.org/10.1038/s41564-021-00899-8.
- Bando, H., Okado, K., Guelbeogo, W.M., Badolo, A., Aonuma, H., Nelson, B., Fukumoto, S., Xuan, X., Sagnon, N., and Kanuka, H. (2013). Intra-specific diversity of *Serratia marcescens* in *Anopheles* mosquito midgut defines *Plasmodium* transmission capacity. Sci. Rep. 3, 1641. https://doi. org/10.1038/srep01641.
- Wang, S., Dos-Santos, A.L.A., Huang, W., Liu, K.C., Oshaghi, M.A., Wei, G., Agre, P., and Jacobs-Lorena, M. (2017). Driving mosquito refractoriness to *Plasmodium falciparum* with engineered symbiotic bacteria. Science 357, 1399–1402. https://doi.org/10.1126/science.aan5478.
- Bai, L., Wang, L.L., Vega-Rodríguez, J., Wang, G.D., and Wang, S.B. (2019). A gut symbiotic bacterium *Serratia marcescens* renders mosquito resistance to *Plasmodium* infection through activation of mosquito immune responses. Front. Microbiol. 10, 1580. https://doi.org/10.3389/ fmicb.2019.01580.
- Jayakrishnan, L., Sudhikumar, A.V., and Aneesh, E.M. (2018). Role of gut inhabitants on vectorial capacity of mosquitoes. J. Vector Borne Dis. 55, 69–78. https://doi.org/10.4103/0972-9062.242567.
- Zhang, R., Neu, T.R., Blanchard, V., Vera, M., and Sand, W. (2019). Biofilm dynamics and EPS production of a thermoacidophilic bioleaching archaeon. N. Biotechnol. 51, 21–30. https://doi.org/10.1016/j.nbt.2019.02.002
- Strathmann, M., Wingender, J., and Flemming, H.C. (2002). Application of fluorescently labelled lectins for the visualization and biochemical characterization of polysaccharides in biofilms of *Pseudomonas aeruginosa*.
 J. Microbiol. Methods 50, 237–248. https://doi.org/10.1016/s0167-7012(02)00032-5.
- Jan, A.T. (2017). Outer membrane vesicles (OMVs) of gram-negative bacteria: a perspective update. Front. Microbiol. 8, 1053. https://doi.org/10.3389/fmicb.2017.01053.
- Schooling, S.R., and Beveridge, T.J. (2006). Membrane vesicles: an overlooked component of the matrices of biofilms. J. Bacteriol. 188, 5945– 5957. https://doi.org/10.1128/JB.00257-06.
- Toyofuku, M., Nomura, N., and Eberl, L. (2019). Types and origins of bacterial membrane vesicles. Nat. Rev. Microbiol. 17, 13–24. https://doi.org/10.1038/s41579-018-0112-2.
- Kamaguchi, A., Nakayama, K., Ichiyama, S., Nakamura, R., Watanabe, T., Ohta, M., Baba, H., and Ohyama, T. (2003). Effect of *Porphyromonas gin-givalis* vesicles on coaggregation of *Staphylococcus aureus* to oral microorganisms. Curr. Microbiol. 47, 485–491. https://doi.org/10.1007/s00284-003-4069-6
- Mukherjee, S., and Bassler, B.L. (2019). Bacterial quorum sensing in complex and dynamically changing environments. Nat. Rev. Microbiol. 17, 371–382. https://doi.org/10.1038/s41579-019-0186-5.
- Fuqua, W.C., Winans, S.C., and Greenberg, E.P. (1994). Quorum sensing in bacteria: the LuxR-Luxl family of cell density-responsive transcriptional regulators. J. Bacteriol. 176, 269–275. https://doi.org/10.1128/jb.176.2. 269-275.1994.
- Waters, C.M., and Bassler, B.L. (2005). Quorum sensing: cell-to-cell communication in bacteria. Annu. Rev. Cell Dev. Biol. 21, 319–346. https://doi.org/10.1146/annurev.cellbio.21.012704.131001.
- Van Houdt, R., Givskov, M., and Michiels, C.W. (2007). Quorum sensing in Serratia. FEMS Microbiol. Rev. 31, 407–424. https://doi.org/10.1111/j. 1574-6976.2007.00071.x.
- Whiteley, M., Diggle, S.P., and Greenberg, E.P. (2017). Progress in and promise of bacterial quorum sensing research. Nature 551, 313–320. https://doi.org/10.1038/nature24624.

Article



- 33. Schuster, M., Sexton, D.J., Diggle, S.P., and Greenberg, E.P. (2013). Acylhomoserine lactone quorum sensing: from evolution to application. Annu. Rev. Microbiol. 67, 43-63. https://doi.org/10.1146/annurev-micro-092412-155635.
- 34. Papenfort, K., and Bassler, B.L. (2016). Quorum sensing signal-response systems in Gram-negative bacteria. Nat. Rev. Microbiol. 14, 576-588. https://doi.org/10.1038/nrmicro.2016.89.
- 35. McClean, K.H., Winson, M.K., Fish, L., Taylor, A., Chhabra, S.R., Camara, M., Daykin, M., Lamb, J.H., Swift, S., Bycroft, B.W., et al. (1997). Quorum sensing and Chromobacterium violaceum: exploitation of violacein production and inhibition for the detection of N-acylhomoserine lactones. Microbiology (Reading) 143, 3703-3711. https://doi.org/10.1099/0022
- 36. Dong, Y.H., Wang, L.H., Xu, J.L., Zhang, H.B., Zhang, X.F., and Zhang, L.H. (2001). Quenching quorum-sensing-dependent bacterial infection by an N-acyl homoserine lactonase. Nature 411, 813-817. https://doi. ora/10.1038/35081101.
- 37. Florez, C., Raab, J.E., Cooke, A.C., and Schertzer, J.W. (2017). Membrane distribution of the Pseudomonas quinolone signal modulates outer membrane vesicle production in Pseudomonas aeruginosa. mBio 8. https://doi. org/10.1128/mBio.01034-17.
- 38. Schertzer, J.W., and Whiteley, M. (2012). A bilayer-couple model of bacterial outer membrane vesicle biogenesis. mBio 3. https://doi.org/10.1128/
- 39. Fineran, P.C., Slater, H., Everson, L., Hughes, K., and Salmond, G.P. (2005). Biosynthesis of tripyrrole and beta-lactam secondary metabolites in Serratia: integration of quorum sensing with multiple new regulatory components in the control of prodigiosin and carbapenem antibiotic production. Mol. Microbiol. 56, 1495-1517. https://doi.org/10.1111/j.1365-2958.2005.04660.x.
- 40. Slater, H., Crow, M., Everson, L., and Salmond, G.P.C. (2003). Phosphate availability regulates biosynthesis of two antibiotics, prodigiosin and carbapenem, in Serratia via both quorum-sensing-dependent and -independent pathways. Mol. Microbiol. 47, 303-320. https://doi.org/10.1046/j. 1365-2958.2003.03295.x.
- 41. Avila-Calderón, E.D., Ruiz-Palma, M.D.S., Aguilera-Arreola, M.G., Velázquez-Guadarrama, N., Ruiz, E.A., Gomez-Lunar, Z., Witonsky, S., and Contreras-Rodríguez, A. (2021). Outer membrane vesicles of gramnegative bacteria: an outlook on biogenesis. Front. Microbiol. 12, 557902. https://doi.org/10.3389/fmicb.2021.557902.
- 42. Schwechheimer, C., and Kuehn, M.J. (2015). Outer-membrane vesicles from Gram-negative bacteria: biogenesis and functions. Nat. Rev. Microbiol. 13, 605-619. https://doi.org/10.1038/nrmicro3525.
- 43. Beveridge, T.J. (1999). Structures of gram-negative cell walls and their derived membrane vesicles. J. Bacteriol. 181, 4725-4733. https://doi. org/10.1128/JB.181.16.4725-4733.1999.
- 44. Kulp, A., and Kuehn, M.J. (2010). Biological functions and biogenesis of secreted bacterial outer membrane vesicles. Annu. Rev. Microbiol. 64, 163-184, https://doi.org/10.1146/annurev.micro.091208.073413.
- 45. Roier, S., Zingl, F.G., Cakar, F., Durakovic, S., Kohl, P., Eichmann, T.O., Klug, L., Gadermaier, B., Weinzerl, K., Prassl, R., et al. (2016). A novel mechanism for the biogenesis of outer membrane vesicles in Gram-negative bacteria. Nat. Commun. 7, 10515. https://doi.org/10.1038/ncomms10515.
- 46. Kassab, E., Fuchs, M., Haack, M., Mehlmer, N., and Brueck, T.B. (2019). Engineering Escherichia coli FAB system using synthetic plant genes for the production of long chain fatty acids. Microb. Cell Fact. 18, 163. https://doi.org/10.1186/s12934-019-1217-7.
- 47. Zhang, Y.M., and Rock, C.O. (2008). Membrane lipid homeostasis in bacteria. Nat. Rev. Microbiol. 6, 222-233. https://doi.org/10.1038/nrmicro1839.
- 48. Comerford, S.A., Huang, Z., Du, X., Wang, Y., Cai, L., Witkiewicz, A.K., Walters, H., Tantawy, M.N., Fu, A., Manning, H.C., et al. (2014). Acetate dependence of tumors. Cell 159, 1591-1602. https://doi.org/10.1016/j. cell.2014.11.020.

- 49. Yao, J., and Rock, C.O. (2015). How bacterial pathogens eat host lipids: implications for the development of fatty acid synthesis therapeutics. J. Biol. Chem. 290, 5940-5946. https://doi.org/10.1074/jbc.R114.636241.
- 50. Hunt, D.W., Winters, G.C., Brownsey, R.W., Kulpa, J.E., Gilliland, K.L., Thiboutot, D.M., and Hofland, H.E. (2017). Inhibition of sebum production with the acetyl coenzyme A carboxylase inhibitor Olumacostat Glasaretil. J. Invest. Dermatol. 137, 1415–1423. https://doi.org/10.1016/j.jid.2016. 12.031.
- 51. Wu, L., and Luo, Y. (2021). Bacterial quorum-sensing systems and their role in intestinal bacteria-host crosstalk. Front. Microbiol. 12, 611413. https://doi.org/10.3389/fmicb.2021.611413.
- 52. Wang, Y., Bian, Z., and Wang, Y. (2022). Biofilm formation and inhibition mediated by bacterial quorum sensing. Appl. Microbiol. Biotechnol. 106, 6365-6381. https://doi.org/10.1007/s00253-022-12150-3.
- 53. Flemming, H.C., Wingender, J., Szewzyk, U., Steinberg, P., Rice, S.A., and Kjelleberg, S. (2016). Biofilms: an emergent form of bacterial life. Nat. Rev. Microbiol. 14, 563-575. https://doi.org/10.1038/nrmicro.2016.94.
- 54. Wang, S., Ghosh, A.K., Bongio, N., Stebbings, K.A., Lampe, D.J., and Jacobs-Lorena, M. (2012). Fighting malaria with engineered symbiotic bacteria from vector mosquitoes. Proc. Natl. Acad. Sci. USA 109, 12734-12739. https://doi.org/10.1073/pnas.1204158109.
- 55. Yazdi, S., and Ardekani, A.M. (2012). Bacterial aggregation and biofilm formation in a vortical flow. Biomicrofluidics 6, 44114. https://doi.org/10. 1063/1.4771407
- 56. McMahon, K.J., Castelli, M.E., García Vescovi, E.G., and Feldman, M.F. (2012). Biogenesis of outer membrane vesicles in Serratia marcescens is thermoregulated and can be induced by activation of the rcs phosphorelay system. J. Bacteriol. 194, 3241-3249. https://doi.org/10.1128/JB.00016-12.
- 57. McBroom, A.J., and Kuehn, M.J. (2007). Release of outer membrane vesicles by gram-negative bacteria is a novel envelope stress response. Mol. Microbiol. 63, 545-558. https://doi.org/10.1111/j.1365-2958.2006.05522.x.
- 58. World Health Organization (2022). World malaria report 2022 (WHO). https://www.who.int/teams/global-malaria-programme/reports/worldmalaria-report-2022.
- 59. Wang, S., and Jacobs-Lorena, M. (2013). Genetic approaches to interfere with malaria transmission by vector mosquitoes. Trends Biotechnol. 31, 185-193. https://doi.org/10.1016/j.tibtech.2013.01.001.
- 60. Tamura, K., Stecher, G., Peterson, D., Filipski, A., and Kumar, S. (2013). MEGA6: molecular evolutionary genetics analysis version 6.0. Mol. Biol. Evol. 30, 2725-2729. https://doi.org/10.1093/molbev/mst197.
- 61. Zhu, J., and Mekalanos, J.J. (2003). Quorum sensing-dependent biofilms enhance colonization in Vibrio cholerae. Dev. Cell 5, 647-656. https://doi. org/10.1016/s1534-5807(03)00295-8.
- 62. Bachurski, D., Schuldner, M., Nguyen, P.H., Malz, A., Reiners, K.S., Grenzi, P.C., Babatz, F., Schauss, A.C., Hansen, H.P., Hallek, M., et al. (2019). Extracellular vesicle measurements with nanoparticle tracking analysis - an accuracy and repeatability comparison between NanoSight NS300 and ZetaView. J. Extracell. Vesicles 8, 1596016. https://doi.org/ 10.1080/20013078.2019.1596016.
- 63. Kumar, S., Molina-Cruz, A., Gupta, L., Rodrigues, J., and Barillas-Mury, C. (2010). A peroxidase/dual oxidase system modulates midgut epithelial immunity in Anopheles gambiae. Science 327, 1644-1648. https://doi.org/
- 64. Wei, G., Lai, Y., Wang, G., Chen, H., Li, F., and Wang, S. (2017). Insect pathogenic fungus interacts with the gut microbiota to accelerate mosquito mortality. Proc. Natl. Acad. Sci. USA 114, 5994-5999. https://doi. org/10.1073/pnas.1703546114.
- 65. Paton, D.G., Childs, L.M., Itoe, M.A., Holmdahl, I.E., Buckee, C.O., and Catteruccia, F. (2019). Exposing Anopheles mosquitoes to antimalarials blocks Plasmodium parasite transmission. Nature 567, 239-243. https:// doi.org/10.1038/s41586-019-0973-1.



STAR***METHODS**

KEY RESOURCES TABLE

REAGENT or RESOURCE	SOURCE	IDENTIFIER
Antibodies		
Anti-Amlip antibody	Gao et al. ¹⁷	N/A
Goat Anti-Mouse IgG H&L (HRP)	Abcam	Cat#ab6789; RRID:AB_955439
Bacterial and virus strains		
Serratia urealytica Su_YN1	Gao et al. ¹⁷	N/A
Su_YN1-mScarlet	This paper	N/A
Su_YN1- Renilla Luciferase	This paper	N/A
Su_YN1-AiiA	This paper	N/A
ΔSuel-Su_YN1	This paper	N/A
Suel-Comp-Su_YN1	This paper	N/A
ΔSueR-Su_YN1	This paper	N/A
Δ <i>paaB-</i> Su_YN1	This paper	N/A
Δ <i>paaJ-</i> Su_YN1	This paper	N/A
Δ <i>paaK</i> -Su_YN1	This paper	N/A
Δ <i>paaH-</i> Su_YN1	This paper	N/A
Δ <i>paaG</i> -Su_YN1	This paper	N/A
Δ <i>pCaF-</i> Su_YN1	This paper	N/A
S. marcescens AS1	Wang et al. ¹⁹	N/A
E.coli DH5α-mScarlet	This paper	N/A
E.coli DH5α- Renilla Luciferase	This paper	N/A
Biological samples		
O-type human blood	Shanghai Red Cross Blood Center, China	Approval number: shblood2019-28
Chemicals, peptides, and recombinant proteins		
RNAiso Plus	Takara	Cat#9109
PrimeScript™ RT reagent Kit	Takara	Cat#RR047A
AceQ qPCR SYBR Green Master Mix	Vazyme	Cat#Q111
AceQ qPCR SYBR Green Master Mix Ac-CoA Synthase Inhibitor1	Vazyme MCE	Cat#Q111 Cat#HY-104032
	•	
Ac-CoA Synthase Inhibitor1	MCE	Cat#HY-104032
Ac-CoA Synthase Inhibitor1 Olumacostat glasaretil	MCE MCE	Cat#HY-104032 Cat#HY-17641
Ac-CoA Synthase Inhibitor1 Olumacostat glasaretil FITC-Con A	MCE MCE MKBio	Cat#HY-104032 Cat#HY-17641 Cat#MP6321
Ac-CoA Synthase Inhibitor1 Olumacostat glasaretil FITC-Con A SYTOX Green N-Hexanoyl-L-homoserine lactone	MCE MCE MKBio Keygentec	Cat#HY-104032 Cat#HY-17641 Cat#MP6321 Cat#KGA261
Ac-CoA Synthase Inhibitor1 Olumacostat glasaretil FITC-Con A SYTOX Green N-Hexanoyl-L-homoserine lactone >=96% (HPLC)	MCE MCE MKBio Keygentec Sigma-Aldrich	Cat#HY-104032 Cat#HY-17641 Cat#MP6321 Cat#KGA261 Cat#56395
Ac-CoA Synthase Inhibitor1 Olumacostat glasaretil FITC-Con A SYTOX Green N-Hexanoyl-L-homoserine lactone >=96% (HPLC) 2-heptyl-3-hydroxy-4(1H)-Quinolone	MCE MCE MKBio Keygentec Sigma-Aldrich GLPBio	Cat#HY-104032 Cat#HY-17641 Cat#MP6321 Cat#KGA261 Cat#56395 Cat#GC45912-5
Ac-CoA Synthase Inhibitor1 Olumacostat glasaretil FITC-Con A SYTOX Green N-Hexanoyl-L-homoserine lactone >=96% (HPLC) 2-heptyl-3-hydroxy-4(1H)-Quinolone C4-HSL	MCE MCE MKBio Keygentec Sigma-Aldrich GLPBio Sigma-Aldrich	Cat#HY-104032 Cat#HY-17641 Cat#MP6321 Cat#KGA261 Cat#56395 Cat#GC45912-5 Cat#SML3427
Ac-CoA Synthase Inhibitor1 Olumacostat glasaretil FITC-Con A SYTOX Green N-Hexanoyl-L-homoserine lactone >=96% (HPLC) 2-heptyl-3-hydroxy-4(1H)-Quinolone C4-HSL DMSO	MCE MCE MKBio Keygentec Sigma-Aldrich GLPBio Sigma-Aldrich Sigma-Aldrich	Cat#HY-104032 Cat#HY-17641 Cat#MP6321 Cat#KGA261 Cat#56395 Cat#GC45912-5 Cat#SML3427 Cat#D2650
Ac-CoA Synthase Inhibitor1 Olumacostat glasaretil FITC-Con A SYTOX Green N-Hexanoyl-L-homoserine lactone >=96% (HPLC) 2-heptyl-3-hydroxy-4(1H)-Quinolone C4-HSL DMSO Effectene transfection reagent	MCE MCE MKBio Keygentec Sigma-Aldrich GLPBio Sigma-Aldrich Sigma-Aldrich Qiagen	Cat#HY-104032 Cat#HY-17641 Cat#MP6321 Cat#KGA261 Cat#56395 Cat#GC45912-5 Cat#SML3427 Cat#D2650 Cat#301425
Ac-CoA Synthase Inhibitor1 Olumacostat glasaretil FITC-Con A SYTOX Green N-Hexanoyl-L-homoserine lactone >=96% (HPLC) 2-heptyl-3-hydroxy-4(1H)-Quinolone C4-HSL DMSO Effectene transfection reagent Giemsa stain, modified	MCE MCE MKBio Keygentec Sigma-Aldrich GLPBio Sigma-Aldrich Sigma-Aldrich Qiagen Sigma-Aldrich	Cat#HY-104032 Cat#HY-17641 Cat#MP6321 Cat#KGA261 Cat#56395 Cat#GC45912-5 Cat#SML3427 Cat#D2650 Cat#301425 Cat#GS500
Ac-CoA Synthase Inhibitor1 Olumacostat glasaretil FITC-Con A SYTOX Green N-Hexanoyl-L-homoserine lactone >=96% (HPLC) 2-heptyl-3-hydroxy-4(1H)-Quinolone C4-HSL DMSO Effectene transfection reagent Giemsa stain, modified Coelenterazine Native	MCE MCE MKBio Keygentec Sigma-Aldrich GLPBio Sigma-Aldrich Sigma-Aldrich Qiagen Sigma-Aldrich Yeasen	Cat#HY-104032 Cat#HY-17641 Cat#MP6321 Cat#KGA261 Cat#56395 Cat#GC45912-5 Cat#SML3427 Cat#D2650 Cat#301425 Cat#GS500 Cat#40904ES02
Ac-CoA Synthase Inhibitor1 Olumacostat glasaretil FITC-Con A SYTOX Green N-Hexanoyl-L-homoserine lactone >=96% (HPLC) 2-heptyl-3-hydroxy-4(1H)-Quinolone C4-HSL DMSO Effectene transfection reagent Giemsa stain, modified Coelenterazine Native L-PHENYLALANINE (13C9, 99%; 15N, 99%)	MCE MCE MKBio Keygentec Sigma-Aldrich GLPBio Sigma-Aldrich Sigma-Aldrich Qiagen Sigma-Aldrich Yeasen Cambridge Isotope Laboratories, Inc.	Cat#HY-104032 Cat#HY-17641 Cat#MP6321 Cat#KGA261 Cat#56395 Cat#GC45912-5 Cat#SML3427 Cat#D2650 Cat#301425 Cat#GS500 Cat#40904ES02 Cat#CNLM-575-H-0.1
Ac-CoA Synthase Inhibitor1 Olumacostat glasaretil FITC-Con A SYTOX Green N-Hexanoyl-L-homoserine lactone >=96% (HPLC) 2-heptyl-3-hydroxy-4(1H)-Quinolone C4-HSL DMSO Effectene transfection reagent Giemsa stain, modified Coelenterazine Native L-PHENYLALANINE (13C9, 99%; 15N, 99%) Acetyl coenzyme A trisodium salt	MCE MCE MKBio Keygentec Sigma-Aldrich GLPBio Sigma-Aldrich Sigma-Aldrich Qiagen Sigma-Aldrich Yeasen Cambridge Isotope Laboratories, Inc.	Cat#HY-104032 Cat#HY-17641 Cat#MP6321 Cat#KGA261 Cat#56395 Cat#GC45912-5 Cat#SML3427 Cat#D2650 Cat#301425 Cat#GS500 Cat#40904ES02 Cat#CNLM-575-H-0.1
Ac-CoA Synthase Inhibitor1 Olumacostat glasaretil FITC-Con A SYTOX Green N-Hexanoyl-L-homoserine lactone >=96% (HPLC) 2-heptyl-3-hydroxy-4(1H)-Quinolone C4-HSL DMSO Effectene transfection reagent Giemsa stain, modified Coelenterazine Native L-PHENYLALANINE (13C9, 99%; 15N, 99%) Acetyl coenzyme A trisodium salt Critical commercial assays	MCE MCE MKBio Keygentec Sigma-Aldrich GLPBio Sigma-Aldrich Sigma-Aldrich Qiagen Sigma-Aldrich Yeasen Cambridge Isotope Laboratories, Inc. Sigma-Aldrich	Cat#HY-104032 Cat#HY-17641 Cat#MP6321 Cat#KGA261 Cat#56395 Cat#GC45912-5 Cat#SML3427 Cat#D2650 Cat#301425 Cat#GS500 Cat#40904ES02 Cat#CNLM-575-H-0.1 Cat#A2056
Ac-CoA Synthase Inhibitor1 Olumacostat glasaretil FITC-Con A SYTOX Green N-Hexanoyl-L-homoserine lactone >=96% (HPLC) 2-heptyl-3-hydroxy-4(1H)-Quinolone C4-HSL DMSO Effectene transfection reagent Giemsa stain, modified Coelenterazine Native L-PHENYLALANINE (13C9, 99%; 15N, 99%) Acetyl coenzyme A trisodium salt Critical commercial assays Acetyl-Coenzyme A Assay Kit	MCE MCE MKBio Keygentec Sigma-Aldrich GLPBio Sigma-Aldrich Sigma-Aldrich Qiagen Sigma-Aldrich Yeasen Cambridge Isotope Laboratories, Inc. Sigma-Aldrich	Cat#HY-104032 Cat#HY-17641 Cat#MP6321 Cat#KGA261 Cat#56395 Cat#GC45912-5 Cat#SML3427 Cat#D2650 Cat#301425 Cat#GS500 Cat#40904ES02 Cat#CNLM-575-H-0.1 Cat#A2056 Cat#MAK039

(Continued on next page)





Continued		
REAGENT or RESOURCE	SOURCE	IDENTIFIER
Deposited data		
Su_YN1 genome sequence data	This paper	NCBI GenBank assembly accession: GCA_017565285.1
Su_YN1 RNA-sequence data	This paper	NCBI SRA data: PRJNA972123
Experimental models: Cell lines		
HEK293T	ATCC	Cat#CRL-3216
Experimental models: Organisms/strains		
Mice: ICR	Shanghai Slack Laboratory Animal Co., Ltd	Slac:ICR
Anopheles stephensi (Dutch strain)	This paper	N/A
Plasmodium falciparum NF54W	This paper	N/A
Plasmodium berghei ANKA	This paper	N/A
Oligonucleotides		
See Table S1 for primers	This paper	N/A
Recombinant DNA		
PSQ	This paper	N/A
oSPC-mScarlet	This paper	N/A
psiCHECK-2 Vector	Promega	Cat#C8021
pTolo-SUMO	This paper	N/A
Software and algorithms		
BLAST	NCBI	https://blast.ncbi.nlm.nih.gov/Blast.cgi
Microsoft Excel	Microsoft	https://www.microsoft.com/zh-cn/microsoft-365/excel
GraphPad Prism 5.0	GraphPad Prism	https://www.graphpad-prism.cn/? c=i&a=prism
Adobe Illustrator CC 2018	Adobe	https://www.adobe.com/cn/products/ illustrator.html
MEGA6.0	Megasoftware ⁶⁰	https://megasoftware.net/ archived_version_active_download
Other		
Filter unit (0.22 μm)	Millipore	Cat#SLGP033RB
Fetal bovine serum	Thermofisher	Cat#10099141C
DMEM	Cytiva-Hyclone	Cat#SH30022.01
RPMI 1640	Corning	Cat#10-041-CV
Bovine Serum Albumin	ABCONE	Cat#A23088
Crystal Violet Staining Solution	Sangon Biotech	Cat#E607309
Phe-deficient RPMI1640 medium	Yichen Bio	Cat#SL0940

RESOURCE AVAILABILITY

Lead contact

Further information and requests for resources and reagents should be directed to and will be fulfilled by the lead contact, Sibao Wang (sbwang@cemps.ac.cn).

Materials availability

All unique/stable reagents generated in this study are available from the lead contact with a completed materials transfer agreement.

Data and code availability

- The transcriptome data have been deposited in the NCBI SRA: PRJNA972123. The bacterial whole-genome sequence data have been deposited in the NCBI GenBank assembly accession: GCA_017565285.1.
- This paper does not report any original code.
- Any additional information required to reanalyze the data reported in this paper is available from the lead contact upon request.



EXPERIMENTAL MODEL AND STUDY PARTICIPANT DETAILS

Mouse models and ethics statement

ICR mice were purchased from Shanghai Slack Laboratory Animal Co., Ltd. Males (ages 6 to 8-weeks) were used in *Plasmodium* infection and mosquito blood feeding. All protocols for animal maintenance, care and experimentation were approved by the Animal Care and Use Committee of the CAS Center for Excellence in Molecular Plant Sciences (Shanghai Institute of Plant Physiology and Ecology) (A01MP2001).

Human blood

The O-type human blood used in this study was sourced from the Shanghai Red Cross Blood Center (Approval number: shblood2019-28).

Mosquito model and rearing conditions

Anopheles stephensi (Dutch strain) mosquitoes were used in the colonization and Plasmodium infection assays in this study. An. stephensi mosquitoes were maintained on 10% sucrose at 27 $^{\circ}$ C and 70 \pm 5% relative humidity (RH) under a 12 h/12 h day-night cycle. Larvae were fed on cat food pellets and ground fish food supplement.

Bacteria strains and growth conditions

The Serratia ureilytica strain Su_YN1 and the Escherichia coli strain DH5α were maintained in Luria-Bertani medium. For Su_YN1 bio-film assays and OMV quantification assays, Su_YN1 and its mutation strains were cultured in RPMI 1640 medium, supplied with or without FBS as stated.

Plasmodium strains and mosquito infection

The *Plasmodium falciparum* strain NF54W (*P. falciparum* NF54W) and *P. berghei* strain ANKA (*P. berghei* ANKA 2.34) were used for mosquito infection. For *P. falciparum* NF54W infection, *in vitro* cultured mature gametocytes were fed to *An. stephensi* mosquitoes. For *P. berghei* ANKA infection, 6-week old ICR (Institute of Cancer Research) mice infected with *P. berghei* ANKA were used for mosquito blood feeding.

Mammalian cell culture

HEK293T cells obtained from ATCC were cultured in DMEM supplemented with 10% FBS at 37°C with 5% CO₂.

METHOD DETAILS

Colonization and quantification of bacteria in the mosquito midgut

Su_YN1 wild type or QS mutants were cultured overnight, harvested by centrifugation at 3,000g for 10 min, washed three times in sterile PBS, and resuspended in 5% sterile sucrose solution to achieve a concentration of 1 \times 10⁷ cells/mL. These bacteria were administered to two-day-old female mosquitoes via soaked cotton pads for 36 h, after which the pads were replaced with sterile cotton pads moistened with 10% sucrose solution. Two days later, the mosquitoes were fed on a blood meal, surface-sterilized with cold 75% ethanol, and their midguts were dissected and homogenized in sterile PBS under sterile conditions 0, 1, 1.5, 2 and 3 days after the blood meal. The bacterial numbers were determined by plating tenfold serial dilutions of the homogenates on LB agar plates supplemented with 100 μ g /mL kanamycin, 100 μ g /mL carbenicillin, followed by incubation at 30 °C for 24 h. The Colony-forming units per mosquito were counted.

Generation of gene disruption, gene complementation, and quorum quenching enzyme expression strains

The quorum sensing (QS) genes in the *S. ureilytica* Su_YN1 strain were deleted using the Red/ET method as previously described. ¹⁷ Briefly, Su_YN1 was transformed by electro-transfection with the PSQ plasmid. The PSQ-carrying Su_YN1 cells were further transformed with recombinant DNA fragments targeting the genomic locus of interest. PCR was used to confirm gene disruption, and two clones of each gene knockout were selected for subsequent experiments. The primer sequences are listed in Table S1.

Complemented strains were generated by electro-transforming a plasmid carrying the disrupted gene into the KO strain. The *Suel* coding region along with its 500-bp 5'untranslated region was amplified. Successful expression of *Suel* complemented strains were confirmed by sequencing.

Quorum quenching enzyme (Bti-AiiA) expression strains were created by electro-transforming a plasmid containing the *AiiA* coding region into the WT strain.

The AiiA coding region was amplified. Successful expression of AiiA coding strains were confirmed by sequencing

Evolutionary relationship of Serratia SueR proteins

The amino acid sequences of Serratia Su_YN1 SueR and its homologs in other Serratia species were searched and recruited using NCBI Blast online tool (https://blast.ncbi.nlm.nih.gov/Blast.cgi). SueR sequence alignment and their phylogenetic relationship was inferred by the Maximum Likelihood tree method using the MEGA6 software. 60

Article



In vitro biofilm assays

The bacterial cultures were adjusted to an OD600 of 0.005 in 10% FBS RPMI 1640 medium and aliquoted in triplicate into 96-well plates containing 0.1 mL 10% FBS RPMI 1640 medium (for quantitation of biofilms using crystal violet stain), or 50 mL Falcon tubes containing 6 mL 10% FBS RPMI 1640 medium with 22 × 22 mm coverslips. The biofilms were formed by incubating the cultures at 30 °C for a specified time period. Biofilm quantitation using crystal violet stain was performed following previously published protocols. Confocal laser scanning microscopy with an LeicaSP8 Confocal Microscope (Leica), and scanning electron microscopy with the Field Emission Scanning Electron Microscopy (Carl Zeiss, Oberkochen, Germany) were performed according to previously published protocols. The Serratia strains were rendered fluorescent for observation under confocal microscopy using the mScarlet protein (a red fluorescent protein) introduced via electro-transformation.

In vivo biofilm assays

Su_YN1 wild type or QS mutants were introduced into adult mosquitoes via sugar meals. After a period of colonization, mosquito midguts were collected and embedded in Epson resin for sectioning. The semi-thin section samples were then treated in 5% Giemsa stain and examined under an optical microscope.

mRNA sequencing and data analysis

RNA-seq analysis was conducted by Majorbio (Shanghai, China) using the Illumina platform. The resulting data were subjected to bioinformatics analysis using Majorbio Cloud Platform and mapped to the Su_YN1 reference genome. Differential gene expression analysis was performed using the DESeq function, with significance set at p < 0.05 and fold change \geq 1.5). Three biological replicates from separate groups were used for RNA-seq analysis.

CV026 biosensor assay

CV026 biosensor assay for detecting short-chain QS signal molecules was conducted with minor modifications to a previously described method. Briefly, LB agar plate was cut into non-contact strips with a sterile blade. 5μ L of the overnight CV026 bacterial solution was inoculated onto the middle of the long strip and left to incubated at room temperature for 60 min. Subsequently, 2μ L of the sample was inoculated at the front end of the long strip. The plates were then incubated at 30° C for 24 h.

Qualitative and quantitative determination of AHL production by liquid chromatography and mass spectrometry (LC-MS/MS)

For bacteria samples: Bacteria were cultured overnight or at specific time points. Subsequently, bacterial cells were subjected to centrifugation at 6,000 rpm for 5 min. Cell-free culture supernatants (50 mL) prepared from the liquid cultures of the AHL-producing strains were acidified to pH 2.0 to prevent further AHL hydrolysis. These acidified supernatants underwent extraction with ethyl acetate (EtAc) twice, using an equal volume each time. The resultant organic phases obtained from extraction were then pooled. The solvent was vacuum evaporated, and the EtAc extracts were dissolved in 50 μ L of HPLC-grade acetonitrile and stored at -20° C.

For mosquito samples: For each group, 5 mosquitoes were dissected, and the midguts were homogenized in 250μ l PBS, then 50μ l homogenates were extracted twice with $500~\mu$ L of EtAc. The extracted organic phases were then pooled, and solvent was vacuum evaporated. The EtAc extracts were finally dissolved in $50~\mu$ L of HPLC-grade acetonitrile and stored at -20° C.

An LC-MS/MS analysis was performed with an Agilent MSD/QTOF 6545 system (Agilent Technologies, Germany) coupled with HPLC/1290II. The aqueous mobile phase A was based on 0.05% acetic acid in H_2O (MS grade), and mobile phase B was based on 0.05% acetic acid in acetonitrile (HPLC grade). The concentrations of solvents A and B ranged from 5 to 75 and 25 to 95%, respectively. The injection volume was 5μ L, and the temperature of the HPLC column was kept at 30°C. Agilent extend 300-C18 HPLC column (4.6 × 150 mm, particle size 3.5 μ m) was used for HPLC separations. The mass spectrometer was set to positive ionization mode with a capillary voltage of 4,000 V, a drying gas (nitrogen) temperature of 300°C, flow rate of 10 L/min, and nebulizer pressure of 20 psi, with nitrogen (99.99%) as the collision gas. The qualitative and quantitative analysis was conducted by Agilent Mass Hunter software (USA). For quantification, the mass spectrometer was configured to monitor specific ions. The selected ions and the respective AHLs are listed below: m/z 172, BHL; m/z 200, HHL; m/z 214, OHHL; m/z 216, HHHL; m/z 228, OHL; m/z 226. The concentrations of AHLs in EtAc extracts of midgut bacterial supernatants are expressed in units of ng/μ L. AHL standards were purchased from Sigma-Aldrich Ltd.

Bacterial culture for OMV preparation

The OMVs were isolated as previously described with minor adaptations. Unless stated otherwise, bacteria were cultured overnight at 30 $^{\circ}$ C in RPMI 1640 (10-041-CV, Corning) with or without 10% FBS (10099141C, Thermofisher). The bacterial cultures were then centrifuged at 4,000 rpm for 20 min, and the resulting supernatants were filtered sequentially through a 0.45 μ m filter (SLHP033RS, Merck) and a 0.22 μ m filter (SLGPR33RB, Merck). The OMVs present in the filtered supernatant were pelleted by ultracentrifugation at 250,000 g for 1 h at 4 $^{\circ}$ C in 26 mL ultracentrifuge tubes (355654, Beckman) using a Beckman 70Ti rotor. The resulting OMV pellets were washed in PBS and subjected to another round of ultracentrifuged. The washed OMV pellets were then resuspended in 1 mL of PBS (for quantification and biochemistry tests) or RPMI 1640 medium (for *Plasmodium* culture tests).



Cell Host & Microbe Article

Bacterial RNA extraction

Bacteria were washed in ice-cold PBS and then transferred to a 1.5 mL microcentrifuge tube containing $500 \,\mu\text{L}$ RNAiso Plus (Takara). Total RNA was extracted from the bacterial cells using the RNAiso Plus protocol according to the manufacturer's instructions. After extraction, the RNA was treated with RNase-free DNase I (Takara) to remove any residual genomic DNA.

Quantitative real-time PCR analysis

Complementary DNA was synthesized from total RNA using a PrimeScript RT reagent kit with gDNA Eraser (Takara), following the manufacturer's instructions. Quantitative real-time PCR analysis was performed with the he AceQ qPCR SYBR Green master mix (Vazyme) on PikoReal 96 (Thermo). Primers are shown in Table S1.

OMV quantification analysis

OMVs were quantified using following different methods.

Nanoparticle tracking analysis (NTA) assay: Nanoparticle tracking analysis of bacteria filtered culture supernatant was performed using NanoSight NS300 instrument (Malvern Panalytical) at 25°C. The movement of particles was analyzed using nanoparticle tracking analysis software following the manufacturer's instructions (NanoSight NS300 User Manual, MAN0541-02-EN, 2018), with the minimal expected particle size, minimum track length, and blur setting all set to automatic. Each video was then analyzed to determine the mean and distribution of OMV size. 62

OMV Protein concentration was determined using BCA Protein Assay (Pierce™ BCA Protein Assay Kit, 23227) and normalized to the OD600 of the respective culture.

Acetyl-CoA inhibitor treated OMV quantification assay: Bacteria were cultured overnight at 30°C in RPMI 1640 + 10% FBS with or without varying doses of Acetyl-CoA inhibitor. OMVs were isolated as described previously. OMV protein concentration was determined using the BCA Protein Assay (Pierce™ BCA Protein Assay Kit, 23227) and normalized to the OD600.

Transmission electron microscopy (TEM) analysis

For midgut samples: The midgut sections were embedded in Epson resin for sectioning. The ultrathin samples were then treated with 2% uranium acetate and lead citrate before being analyzed using a Hitachi TEM (model no. H-7700).

For OMV samples: A total of 3 μ L of the OMV preparations were placed on carbon-coated copper grids (Cat# BZ10021b, ZJKY) and allowed to absorb for 3 min. The excess liquid was then removed, and the samples were negatively stained with 2% (wt/vol) uranyl acetate for 3 min before being evaluated using TEM.

For bacteria samples: The parasites were washed with PBS and centrifuged at 1,000 g for 3 min. The cell pellets were fixed in 2.5% glutaraldehyde and then sectioned for TEM analysis.

Expression and purification of SUMO-SueR

Small ubiquitin-like modifier (SUMO)-SueR protein was purified from *E. coli* strain BL21 DE3 strain by inducing expression with 100 μM IPTG, resulting in soluble form. The protein was then purified using the Ni-NTA resin. The proteins were eluted with 300 mM imidazole, and then dialyzed in PBS buffer (pH 7.4). The protein concentration was determined using the BCA assay, while SDS-PAGE was used to assess the protein's purity.

Protein extraction and western blot analysis

Protein extraction from mosquito midguts was performed using RIPA buffer supplemented with a complete protease inhibitor cocktail. After ultrasonication, the protein solution was centrifuged at 12,000g for 10 min at 4 °C, and the resulting supernatant was collected. Laemmli sample buffer was added to the collected supernatant, which was then fractionated by 10% SDS–PAGE and transferred onto a PVDF membrane. The membrane was blocked in blocking buffer (5% BSA in 1×TBST, Tris-buffered saline and Tween 20) and then incubated with primary antibodies. After incubation, the membrane was washed three times with TBST and incubated with HRP-conjugated secondary antibodies. The membrane was washed four times in TBST before enhanced chemiluminescence detection.

Electrophoretic mobility shift assays (EMSAs)

A 300 bp DNA probe targeting the promoter region of the phenylalanine metabolic gene cluster was prepared by PCR and labeled with Cy5. The purified SueR protein was incubated with the Cy5-labeled DNA probes and C6-HSL in 20 μ L of binding buffer containing 100 mM Tris, 25% Glycerin, 0.2 mg/mL BSA, 0.01 M MgCl₂, 0.00025 M DTT, and 2 μ g Fish Sperm DNA. The mixture was incubated at 25°C for 20 min before being separated using 6% polyacrylamide gel electrophoresis in 0.5 × TBE (Tris/boric acid/EDTA) buffer at 0°C and 100V for 100 min. The blots were then visualized using a chemiluminescent detection device (AMERSHAM TYPHOON5).

Luciferase reporter assays

To achieve high transfection efficiency and minimize background expression of phenylalanine metabolic gene cluster promoter, the mammalian HEK293T cell line was used for luciferase reporter assays. The cells were cultured in DMEM high glucose medium (Hy-Clone) supplemented with 10% (vol/vol) heat-inactivated fetal bovine serum (FBS, Gibco) and 1 × antibiotic–antimycotic (Gibco) at

Article



37 °C under 5% CO₂. The ~300 bp sequences flanking the phenylalanine metabolic gene cluster promoter regions or the promoter regions combined with SueR regions, were separately cloned into the *Not*I and *MIu*I sites of the psiCheck-2 vector (Promega). The HEK293T cells were transfected with 100 ng DNA of psiCheck-2 reporters with or without C6-HSL using Attractene Transfection Reagent (Qiagen). After 24 h, cells were harvested and lysed, and the activities of firefly and Renilla luciferases were measured using the Dual-Luciferase Reporter Assay System (Promega). Each sample was tested in triplicate, and transfections were repeated twice.

Acetyl-CoA and ATP measurement

Acetyl-CoA levels were quantified using the Acetyl-CoA Assay Kit (Sigma, MAK039-1KT) following the manufacturer's instructions. Cultured bacteria were lysed by homogenization with 1.0 M perchloric acid, and the lysate then centrifuged at 10,000 × g for 10 min to remove any insoluble material. The resulting supernatant was neutralized with 3 M potassium bicarbonate solution while maintaining the pH between 6 and 8. The Acetyl-CoA levelswere measured using a premade reaction mixture provided in the kit. Furthermore, the ATP content was determined using the Enhanced ATP Assay Kit (Beyotime Biotechnology, Shanghai, China) according to the manufacturer's instructions.

[13C] Acetyl-CoA measurement

The wild type or mutant bacterial cells were cultivated in shake flasks containing L-Phenylalanine-deficient RPMI1640 medium supplemented with 10% dialyzed-FBS and $1\mu M$ ¹³C-labeled L-Phenylalanine (Cambridge Isotope Lab). The bacterial cells were harvested at various time points. Acetyl-CoA was extracted using lysis buffer (methanol: isopropanol = 1:1) and analyzed by LC-MS/MS.

Human blood and P. falciparum gametocyte culture

The O-type human blood was obtained from the Shanghai Red Cross Blood Center (Approval number: shblood2019-28). Red blood cells and serum were used to culture *Plasmodium falciparum* NF54W asexual parasites and gametocytes. *P. falciparum* gametocytes were cultured as previously described.⁶³

In vivo anti-ookinete formation assay of P. falciparum

An. stephensi mosquitoes carrying Su_YN1 wild type or the QS mutants were fed with mature *P. falciparum* NF54W gametocytes. The mosquito midguts were dissected 20 h after the blood feed. The blood bolus was spread on a glass slide and stained with Giemsa. Ookinetes in the midgut of individual mosquitoes were counted under microscopy.

Effect of bacteria on P. berghei infection in mosquitoes

Bacteria were grown overnight in LB broth medium, then washed three times with sterile 1×PBS, and resuspended in 5% (wt/vol) sterile sucrose solution to obtain a concentration of 1 × 10⁷ cells/mL. The bacterial suspension was applied onto sterile cotton pads and used to feed to female mosquitoes as described previously. ⁶⁴ Different groups of mosquitoes were allowed to feed on the same *P. berghei*-infected mouse for 10 min, and were subsequently maintained at 19 °C and 80% relative humidity. Fully engorged mosquitoes were separated within 24 h and provided with a cotton pad soaked with 5% (wt/vol) sterile sucrose solution. Midguts were dissected on day 7 after the blood meal, stained with 0.1% (wt/vol) mercurochrome, and examined for the presence of oocysts.

Exposing C6-HSL to mosquitoes for P. berghei transmission-blocking assay

To perform the *P. berghei* transmission-blocking assay, the mosquitoes were exposed to C6-HSL-treated Petri dishes as previously described. Briefly, C6-HSL (N-Hexanoyl-L-homoserine lactone) stock solution (10mg/mL) was prepared in acetone and then diluted in acetone to obtain a final working concentration. To generate a C6-HSL-coated surface, 1 mL of acetone solution containing 100 ng, and 500 ng C6-HSL was separately added to a 6-cm diameter Petri dishes, resulting in final concentrations of 17.73, and 88.67 nmol/m², respectively. As a control, glass petri dishes were coated with an equal volume of acetone. The treated dishes were then placed on a lateral shaker and allowed to air-dry for 1 h at room temperature. The process coated the compound onto the glass substrate. A translucent glass cup was placed over the coated surface to contain mosquitoes during exposure. For the exposure step, 15–25 Su_YN1-caryying mosquitoes were introduced and incubated on the treated surface for 30 min. The exposure plates were agitated once during exposure to discourage resting on the untreated walls and base of the cup. After exposure, the mosquitoes were transferred to a clean mosquito cup for *P. berghei* infection assay.

QUANTIFICATION AND STATISTICAL ANALYSIS

The statistical significance of the difference in oocyst or ookinete intensities between two treatments was analyzed using the Mann-Whitney test. Other statistical significance was calculated using a two tailed Student's t-test for unpaired comparisons between two groups, or one-way analysis of variance (one-way ANOVA) between more than two groups or two-way analysis of variance (two-way ANOVA) between more than two groups. A value of P < 0.05 was considered to be statistically significant. All statistical analyses were performed using GraphPad Prism version 5.00 for Windows (GraphPad Software).